Early Evolution of Disk Galaxies : Formation of Bulges in Clumpy Young Galactic Disks

Masafumi Noguchi
Astronomical Institute, Tohoku University, Aoba-ku, Sendai 980-77, Japan;
noguchi@astroa.astr.tohoku.ac.jp

ABSTRACT

A new idea is proposed for the origin of bulges in spiral galaxies. Numerical simulations for the protogalactic collapse suggest strongly that galactic bulges have been assembled from massive clumps formed in the galactic disks in their early evolutionary phase. These clumps result from the gravitational instability of the gas-rich disks of young galaxies. Those massive clumps, individual masses of which can be as large as $\sim 10^9 M_\odot$, are able to spiral toward the galactic center owing to dynamical frictions within a few Gyr. Inward transport of disk matter by this process leads to the formation of a galactic bulge. A simple analytical model has been constructed, in which the clumpy evolution of a disk galaxy is controlled by two parameters; the timescale with which the primordial gas in the halo accretes onto the disk plane (i.e., collapse timescale) and the mass fraction of the primordial gas relative to the galaxy total mass. Under plausible assumptions for the variation of these parameters among spiral galaxies, the clumpy evolution model can explain the observed trend that the bulge-to-disk ratio increases as the total mass or the internal density of the galaxy increases. This success suggests that the clumpy evolution of the galactic disk constitutes an important ingredient of the disk galaxy evolution. Star formation in primeval disk galaxies takes place mostly in the clumps. Resulting knotty appearance of these systems may explain the peculiar morphology observed in a number of high-redshift galaxies.

Subject headings: galaxies:formation– galaxies:evolution– galaxies:kinematics and dynamics– galaxies:structure– galaxies:ISM

1. Introduction

One of the most notable structural features of disk galaxies is that they are composed of two distinct components; disks and bulges. The origin of this two-component structure

remains unclear, although it constitutes an important back-bone of disk galaxies. Several theoretical studies have addressed this problem (e.g., Larson 1976, Gott and Thuan 1976). Conventional understanding is that the galactic bulges have been formed as a single body within a relatively short period, as a result of the collapse of a gaseous protogalaxy, and the later accretion of the residual primordial gas has built the disk components. Pioneering models by Larson (1976) for the formation of disk galaxies are one of the most extensive numerical models which have embodied this idea, but have a potential problem that two different regimes of star formation should be assumed in order to realize distinct separation between a bulge and a disk. Recent observations of the Milky Way bulge (e.g., Rich 1996, McWilliam and Rich 1994) and bulges of other galaxies have stimulated attempts to elucidate when and how the galactic bulges have been formed and nature of the bulges itself (e.g.,Matteucci and Brocato 1990, Peletier and Balcells 1996, Kormendy 1993).

On the other hand, recent observations by the Hubble Space Telescope (HST) and other new generation ground-based telescopes are revealing the properties of distant galaxies at the epochs when the Universe was younger than half of its present age, and thus providing a direct access to the initial evolution phase of galaxies. Those galaxies having a redshift $z >\sim 1$ generally exhibit morphologically peculiar structures which defy the application of the traditional Hubble classification scheme (e.g., van den Bergh et al. 1996, Abraham et al. 1996, Glazebrook et al. 1994, Glazebrook et al. 1995, Griffiths et al. 1994, Driver et al. 1995, Cowie et al. 1995). The most remarkable class of those high-redshift galaxies includes the systems which consist of a few blobs (clumps) embedded in a common diffuse envelope. For example, Griffiths et al. (1994) note several galaxies with prominent bright knots in their sample of HST Medium Deep Survey. Galaxies having similar morphology are also found in images examined by other groups (e.g., Giavalisco et al. 1996b, Koo et al. 1996, van den Bergh et al. 1996).

Some of the peculiarities observed in these high-redshift galaxies may originate in copious interstellar gas existing in early evolution phase of disk galaxies. In most disk galaxies which we observe in the present-day universe, the interstellar gas can be regarded as a *dynamically* passive component because of the small fraction it occupies in the total mass of the galaxy. The motion of the gas is determined practically by the gravitational field arising from the stellar component, and apart from dissipative process and star formation, ballistic motion is a good approximation for the description of the gas kinematics. This situation, however, changes drastically if the mass fraction of the gas relative to the total galaxy mass exceeds about 10 percent. In this gas-rich regime, the interstellar gas is very active *dynamically*. The gas, being dissipative and self-gravitating, tends to form numerous massive clumps, each of which is gravitationaly bound. These massive clumps are involved with various dynamical processes (Noguchi 1998). For example, they deflect

stellar motions effectively and heat up the stellar disk component (i.e., increase the stellar velocity dispersion), and thus affect the stability of the galactic disk (Shlosman and Noguchi 1993, Noguchi 1996). Noguchi (1998) has proposed the gravitational instability origin for those sub-galactic clumps frequently observed in high-redshift galaxies, and argued that they may serve as building blocks of galactic bulges. The present paper expands upon this idea and tries to discuss the evolution of young disk galaxies in more details, with much emphasis placed on the formation of galactic bulges and dependence of its efficiency on galaxy parameters.

§2 and §3 describe the numerical simulation which has inspired the new idea of bulge formation. In §4, an analytical modelling is devised for the growth of galactic disks and is applied to bulge formation. Observational data about global properties of spiral galaxies are summarized in §5, and compared with the theoretical results in §6. Discussion and conclusions are given in §7 and §8, respectively.

2. Numerical Simulation

This section provides a full account of the numerical model which has motivated the new idea of bulge formation briefly given in Noguchi (1998) and examined extensively here. Collapse of a protogalaxy composed of the dark matter and primordial gas has been simulated by an N-body method including a star formation algorithm. Similar approaches have been taken by many researchers (e.g., Baron and White 1987, Katz and Gunn 1991, Katz 1992, Steinmetz and Müller 1995, Navarro and White 1994). Unlike most of these works, which employed initial conditions based on a specific type of cosmology such as the Cold Dark Matter model, the present work does not assume a particular cosmology. I start from an idealized initial condition and attempt to predict properties of young disk galaxies which will be robust to the nature of the assumed cosmology. The primary interest here is in investigating detailed morphological and dynamical evolution of forming disk galaxies. Therefore the simulation is restricted to a three dimensional volume which encloses a single galaxy. The factor by which a galaxy has collapsed after turn-around (i.e., separation from Hubble expansion) is considered to be large, a factor of 10 (e.g., Fall and Efstathiou 1980). The present study does not deal with the whole process of this collapse but only the evolution of the galaxy after it has shrinked to the present size and has become balanced by the increased centrifugal force in the direction perpendicular to the rotation axis. Therefore, the halo (the dark matter) mentioned hereafter means only its portion contained in the optical radius of the galaxy. This limitation in space makes it possible to investigate more detailed structure and kinematics of the forming galaxy than other

cosmologically-implemented simulations.

The primordial gas which has been destined to make the visible parts of the present-day galaxies is considered to have been more-or-less clumpy (e.g., Fall and Rees 1985). Sizes and masses of these clumps are matter of debate. Though the recent progress in the observational technique is enabling access to these pregalactic entities, in the form of quasar absorption line systems for example, the physical properties deduced from those observations are diverse. For example, Steidel (1990) estimates the typical size of 1 - 15 kpc and the mass of $10^6 - 10^9 M_\odot$ for the Lyman limit systems, which are considered to constitute halos of galaxies located on the line-of-sights to more distant quasars.

Depending on the assumed size and mass of these building blocks, two extreme pictures can be considered to describe the formation process of galaxies in general. The first one envisions a relatively regular and smooth (both spatially and temporarily) gas accretion process in the potential well of the protogalaxy (e.g., Gott and Thuan 1976, Larson 1976). Graininess of the pregalactic clumps is neglected on the scale of galaxy size. The second picture, in another extreme, considers that a typical galaxy has been made by mergers of subgalactic units, which are not so small and numerous as to permit neglect of their discreteness (e.g., Cole et al. 1994).

Although the evolution of elliptical galaxies could be much different depending on which picture is adopted, these two limiting scenarios seem to converge in the case of disk galaxies. Stellar dynamical processes, which retain memory of initial conditions to some extent, are considered to have non-negligible effects on the formation and evolution of elliptical galaxies. In contrast with this, the observed thiness of the galactic disks suggests that the assembling of pregalactic units into galactic disks has been a highly dissipative process. Merger of non-dissipative stellar systems would puff up the disk (e.g., Tóth and Ostriker 1992). In other words, pregalactic bodies, whatever their sizes and masses may have been, should have been primarily gaseous when they coagulated to make a galactic disk. Dissipative nature of these bodies must have erased identity of individual bodies quickly. Thus, all the disk galaxies, in their early evolutionary phase, should have had a relatively smooth and mostly gaseous galactic disk with roughly the same radius and thickness as the present-day stellar disk, both in the smooth collapse picture and in the merger scenario.

2.1. Initial Conditions

As a device to realize dissipative growth of a galactic disk, we consider a spherical protogalaxy consisting of dark matter and primordial gas. These two components have uniform density distributions with the same cut-off radius, $R = 15kpc$. The total mass of the system is $M = 1.5 \times 10^{11} M_{\odot}$, with the masses of the dark matter and gas components being $M_h = 0.75 \times 10^{11} M_{\odot}$ and $M_g = 0.75 \times 10^{11} M_{\odot}$, respectively. With this choice, the dynamical timescale of the system, $(R^3/GM)^{1/2} = 7.06 \times 10^7 yr$, where G is the gravitational constant. The unit velocity becomes $(GM/R)^{1/2} = 208 kms^{-1}$. The dark matter and gas components are modeled as systems comprising $N_h = 20000$ and $N_g = 30000$ particles, respectively. The adopted gas fraction, $M_g/M = 0.5$, is based on the observations that the mass fraction of the dark halo component *within the optical radius* is clustering around 0.5 for most disk galaxies for which the rotation curve and the distribution of the luminous component are observed with high accuracy (van der Kruit and Searle 1982, Bahcall and Casertano 1985, but see also discussion in §4.6). There is no stellar particle initially (N_s=0).

The dark matter particles are given isotropic random motions with an one-dimensional velocity dispersion of $\sigma = 122 kms^{-1}$, bringing the dark halo into virial equilibrium roughly. The gas particles are given a uniform rotation with an angular frequency of $\Omega = 13.9 kms^{-1} kpc^{-1}$. Therefore, the gas system is already in rough centrifugal equilibrium owing to enough rotational support, and is expected to collapse not much in the radial direction but mostly along the spin axis. The direction of the angular momentum vector for this rotational motion is taken as the z-axis hereafter, with the x- and y- axes lying in the plane perpendicular to the z-axis. The evolution of the system under its self-gravity is simulated by an N-body method.

The dark matter particles are treated as collisionless. Namely, their motions are determined solely by the global gravitational field they feel. On the other hand, gas particles are modeled as particles which collide with each other inelastically, thus dissipating their kinetic energy. Star formation process from the gas is also included as described shortly. The gravitational force exerted on each particle is calculated by the GRAPE, which is a dedicated device for N-body calculations (Ebisuzaki et al. 1993). The softening radii, $\varepsilon_h = 300pc$ and $\varepsilon_g = 150pc$, are introduced for dark matter and gas particles, respectively, to suppress undesirable two-body effects.

2.2. Gas Dynamics and Star Formation

Gas dynamics is treated by the so-called sticky particle method. Inelastic collisions between the gas particles are introduced to model the dissipative nature of the interstellar medium (Levinson and Roberts 1981, Roberts and Hausman 1984, Hausman and Roberts 1984). All the cloud particles are assumed to have the same finite radius $r_c = 38pc$. In the simulation, two overlapping clouds are made to collide inelastically provided that they are approaching each other. After collision, the radial component of the mutual velocity is multiplied by $f_{col} = 0.01$ and its sign is reversed, while the tangential component is unchanged, in order to mimick energy dissipation. The evolution of the system does not change appreciably as far as $f_{col} <\sim 0.5$.

The star formation process is simulated by changing a gas cloud particle to a stellar particle. This conversion is performed with a probability which is related to the local gas density around the cloud particle as follows. The local gas density, ρ, for a given cloud particle is determined by counting the number of the gas clouds residing in the sphere of a radius $r_{dens} = 750pc$ centered on the cloud in question. Then the probability, p, for star formation for this cloud in the current time step is calculated by, $p = K_{star} \times dt \times \rho^{1/2}$. Here, K_{star} is a coefficient which controls the star formation efficiency, and dt is the size of the time step, which is $7.06 \times 10^5 yr$ (i.e., one hundredth of the dynamical time). The value of K_{star} is determined empirically so that the time variation of star formation rate is in a rough agreement with the one inferred for disk galaxies from various observational data (see §3). The square root dependence on the local gas density expressed in the above expression for p is specified by the consideration that the star formation process, though its detailed nature is not well understood, originates in some form of local gravitational instability in the interstellar medium, and hence its characteristic timescale must be related to the free-fall timescale of the local unstable region.

After getting p by the above equation, one number ξ is created in the range (0,1) using the uniform random number generator. If $\xi < p$, that cloud particle is changed into a stellar one. If $\xi > p$, no such transformation is made. This recipe for star formation, namely converting a whole cloud into a stellar particle with some probability instead of converting some fraction (p in this case) of one cloud at every time step, was taken to avoid intolerable increase of the number of particles in the model as new stars form. This procedure makes the sum of the number of gas particles, N_g, and that of stellar particles, N_s, to be constant during the course of simulation. One important addition to this recipe is specification of a threshold density for star formation. Star formation is inhibited if the local gas density is less than a critical value ρ_{th} (see below). Stellar particles are treated as collisionless, with a gravitational softening parameter, $\varepsilon_s = 150pc$.

The threshold density was set to be $\rho_{th} = 0.1$ ($M_\odot pc^{-3}$). Observations of nearby disk galaxies suggest that the threshold *surface* gas density, μ_{th}, for star formation is $\sim (1-10) M_\odot pc^{-2}$ (Kennicutt 1989). Because the gas in the present model occupies a three-dimensional volume in general and is not necessarily confined in a planar configuration, the application of a surface density sounds questionable and a threshold *volume* density will be more relevant. Using the observed thickness, $h_g \sim 100$ pc, of the distribution of the interstellar molecular gas in the disk of the Milky Way galaxy (e.g., Solomon et al. 1979), I converted the threshold surface density to the threshold volume density like $\rho_{th} \sim \mu_{th}/h_g \sim (0.01-0.1) M_\odot pc^{-3}$. The value adopted for ρ_{th} in the present simulation is the upper limit of this range, though such a translation from the two-dimensional density to a three-dimensional one may not be justified fully, because the configuration of the interstellar matter could affect its stability and ability to form stars.

3. Numerical Results

Morphological evolution of this model is shown in Figure 1. As a galactic disk builds up by infall of the gas from the halo region, several massive clumps are formed in the disk plane [$\sim 0.6 < t < \sim 0.7$, especially Figure 1(e)]. These clumps follow the global rotation of the galactic disk. Some of these clumps are observed to merge and make larger clumps while orbiting in the disk, as clearly seen in Figure 1(e). Because these clumps suffer from dynamical friction against surrounding disk material, they gradually sink to the central region of the disk. This transfer of matter leads to an accumulation of a large mass in the central region. The side view of the system is quite intriguing [Figure 1(f)]. It is noted that this inward motion of clumps leads to the formation of a spheroidal component in the galactic center. It is natural to regard this component as a galactic bulge. Note that almost all the star formation takes place in the disk plane [Figure 1(d)]. The bulge component is not made by early star formation occuring in a spheroidal space at the galactic center.

The clumpiness of the system makes definition of the galactic center not a trivial problem. In the analyses described below, the galactic center is defined to be the center of the most massive clump at each epoch, which is called the bulge. The galactic center thus defined can be displaced from the coordinate origin, $x = y = z = 0$. The mean disk plane, defined as the peak position in the z-distribution of the gas clouds, also drifts slightly in the negative z-direction during the simulation. These deviations from the coordinate system are taken into account in the analysis when appropriate.

Specification of a threshold gas density for star formation is definitely responsible for the lack of star formation before the epoch of disk formation. Volume density of the gas is

very low when the gas occupies a three-dimensional spherical volume of the halo region, but increases by a large amount when the gas is gathered into a two-dimensional disk configuration. This change of the dimensionality initiates vigorous star formation in the galactic disk. On the other hand, the column density of the gas hardly changes because the collapse occurs mostly in the vertical direction.

Clumpiness observed in the numerical model is a direct consequence of the gas-richness of the disk which forms by a relatively rapid infall. Time evolution of the masses of the total disk and the gas disk is shown in Figure 2. Here, the gas particles whose distance from the mean disk plane is less than 0.1 R are considered to constitute the gas disk, and all the stellar particles are regarded as members of the stellar disk. The regions with the cylindrical radius $r < 0.3R$ or $r > 1.5R$ are excluded. Initial evolution is the growth of a mostly gaseous galactic disk along the line $f_g = f_d$. After the disk formation has been almost completed, star formation starts to deplete the gas component, with the model point going down nearly along the line, f_d= constant, in the left panel. A slight decrase in f_d is due to inflow of the clumps toward the galactic center, which builds up the bulge component.

The clumps in this numerical model start to appear distinctly at $t \sim 0.6$ Gyr, when the value of f_g is around its maximum of 0.19. I selected a few typical clumps at $t = 0.64$ Gyr as shown in Figure 1(e) and investigated their internal structure. Examination of the surface density profile made it possible to draw a boundary between the main body of the clump and its envelope and to calculate the mass of the main body as the clump mass. Masses of individual clumps are found to be of the order of $0.01M$ ($\sim 10^9 M_\odot$). This value far exceeds those of any molecular complexes observed in nearby galaxies (i.e., the most massive known entities which constitute the galactic disks in the present epoch), and can be well compared to the masses of dwarf galaxies.

The dashed line in Figure 2 indicates the evolutionary track of an analytical model which is described later. This analytical model, with a collapse timescale of 0.3 Gyr and an initial fraction of the gas mass of 0.5, represents the behavior of the numerical model fairly well. I calculated the expected clump mass as the instantaneous Jeans mass in the growing model disk of this analytical model (open circles in Figure 2, right panel). The clump mass thus obtained reaches the maximum value of $\sim 10^9 M_\odot$ at $t \sim 0.5$ Gyr when f_g (dashed line) reaches the maximum of ~ 0.14, which is roughly equal to the maximum of f_g in the numerical model. The agreement between the numerical and analytical clump masses suggests that the seeds of those clumps in the numerical model are created by the local gravitational instablility in the gaseous disk component. We should, however, be careful in relating the clump mass to the Jeans mass in the disk at current epoch, because masses of

individual clumps in the numerical model increase continuously in general due to mergers among themselves and later accretion of the surrounding gas, whereas the analytically calculated clump mass starts to decrease as f_g decreases.

Figure 3 shows the time development of the star formation rate (SFR). The SFR starts to increase abruptly ~ 0.5 Gyr after the start of the simulation, and attains a peak rate of $\sim 40 M_\odot yr^{-1}$ at $t \sim 0.7$ Gyr. This is just the epoch when most of the gas has settled to the disk [see Figure 1(b)]. The SFR declines after the maximum monotonically except a few weak but distinct burst-like increases. By $t = 2.1$ Gyr, 37 percent of the gas has been converted into stars. The peak SFR of $\sim 40 M_\odot yr^{-1}$ is within the range of 4-75 $M_\odot yr^{-1}$ deduced by Steidel et al. (1996b) for a population of $z > 3$ galaxies. The temporal change of the SFR in the numerical model agrees also with the history of star formation in early-type disk galaxies inferred from the observations (Sandage 1986). Note also that the overall behavior of the SFR is similar to that of the SFR obtained in the analytical model.

It is noted that the SFR reaches the maximum roughly at the time when the clumpy structure is most prominent (Figure 3). This means that, during the course of evolution, the model galaxy will be observed as a clumpy object at the highest probability, provided the observation is made in the rest-frame UV band, which is sensitive to young massive stars. Also note global asymmetry of the stellar component in the present model, which is most noticeable at t= 0.9 Gyr to 1.3 Gyr [see Figure 1(e)].

The asymmetric and clumpy disk seen in this model is strongly reminiscent of the images of many galaxies at large redshift obtained by the HST (e.g., van den Bergh et al. 1996, Griffiths et al. 1994, Koo et al. 1996). Although the irregular and clumpy nature is most noticeably found in the objects with a medium redshift (i.e., $\sim 0.5 < z <\sim 1$), it may be traced into a larger redshift. Steidel et al. (1996a) investigated the morphology of Lyman break galaxies with $2.3 < z < 3.4$ found in the Hubble Deep Field and noticed some objects having multicomponent structure. They also mention diffuse asymmetric "halos" around these high-redshift galaxies. In view of the present numerical result, some parts of these morphological peculiarities may be caused by gravitational instability of the galactic disks in their early evolution phases.

The clumps discussed above experience strong dynamical friction owing to their large masses. Resulting accumulation of clumps to the galactic center makes a bulge as already stated. The bulge in the present numerical model is not formed quickly in a single event as the protogalaxy collapses to the galactic center but is assembled gradually as individual clumps formed in the disk plane spiral into the galactic center. The growth of the bulge is stepwise because accretion of clumps takes place in a discrete manner. Figure 4 shows the distribution of the age for the bulge stars at several epochs. Discrete nature of the

bulge growth is manifested as a few local maxima in the age distribution (see the bottom panel, especially), which correspond respectively to starbursts triggered by the falling-in of a massive clump into the bulge region. At the final epoch indicated ($t = 1.98$ Gyr), the age spread is as large as ~ 1 Gyr.

4. Analytical Multi-Component Models

The numerical model discussed above is enlighting, but has a difficulty. As shown below, one of the most important parameters which govern the evolution of disk galaxies is the accretion timescale, namely, the timescale of gas infall from the halo. It is difficult to vary this timescale freely by employing the sticky-particle method. Accretion can be accelerated or slowed down by varying the size of the clouds and/or the restitution coefficient f_{col} in the cloud collisions in the sticky-particle model. However, it is not fully clear how these parameters are related to the observed properties of the interstellar gas. For example, the giant molecular clouds of the Milky Way galaxy have a very complicated internal structure comprising many hierarchical levels in spatial scale, and no single spatial scale seems to dominate (e.g., Henriksen 1991). Also, the accretion of gas to the disk plane is likely to be affected by other effects than dissipative cloud-cloud collisions as discussed below. These considerations have motivated development of analytical models which introduce the accretion timescale as a free parameter. In this section, I discuss the analytical model of disk growth to remedy the limitation possessed by the numerical simulation. The analytical model developed here has essentially the same ingredients as the previous version described in Noguchi (1996), but is improved in several respects.

4.1. Basic Equations

I consider a spherical halo with a radius R. The primordial gas initially distributed in this halo region gradually accretes to the disk plane and builds up a galactic disk. As the accretion proceeds, the disk becomes to contain more and more gas (i.e., the interstellar gas) and stars form from it. I assume that the stars and the gas in the disk occupy a flat cylindrical region with the same radius as the halo. The whole system considered here is meant to represent the portion of a disk galaxy within its optical radius so that the halo in the present model should be regarded as not representing the entire dark halo (the massive halo) but its portion within the optical extent of the galaxy, in accordance with the numerical model presented above. The system is divided into four components; the halo, the stellar disk, the gas disk, and the bulge. The mass of each component is denoted by m_h,

m_s, m_g, and m_b, respectively. Total mass is denoted by M ($=m_h + m_s + m_g + m_b$). I am not concerned with any structures which might develop in each component but treat each component as a single zone. Namely, the physical state of each component at a given time is specified by several global quantities whose value should be understood as a characteristic one, namely the average over the entire region of that component.

Under this simplification, time evolution of masses in respective components is formulated as follows.

$$\frac{dm_g}{dt} = -SFR - \frac{m_g}{\tau_{fri}} + \frac{M\Gamma t}{\beta^2} exp(-\frac{t}{\beta}), \tag{1}$$

$$\frac{dm_s}{dt} = SFR, \tag{2}$$

and

$$\frac{dm_b}{dt} = \frac{m_g}{\tau_{fri}}, \tag{3}$$

where t is the time reckoned from the beginning of gas infall (which is here assumed to be 12 Gyr ago). The first term in the righthand side of equations (1) and (2) denotes the effect of star formation and SFR here stands for the star formation rate for the whole galaxy. τ_{fri} is the timescale of the inward motion of clumps formed in the disk. This inflow is caused by dynamical frictions acting upon the clumps, and its timescale determines the growth rate of the bulge component. The bulge growth is determined by eq(3) in this analytical formulation. The third term in the righthand side of equation (1) represents addition of gas to the disk by the accretion (gas infall) from outside the disk plane, the timescale of which is denoted by β. Hereafter, β is referred to interchangeably as the accretion timescale, the collapse timescale, or the infall timescale. As the infall proceeds, the mass of the halo decreases correspondingly, because the total mass of the system, M, is assumed to be conserved (Here the halo serves only as a reservoir of the primordial gas and its evolution is not traced). The total mass of the matter which eventually accretes to the disk is specified by its fraction, Γ, with respect to the total mass of the galaxy. Namely, Γ is the fraction of the gas mass relative to the total galaxy mass at the initial instant. The functional form of the time variation of the infall rate in eqation (1) was adopted because it is physically reasonable and mathematically convenient. The time dependence here is slightly modified from the previous one adopted in Noguchi (1996).

4.2. Star Formation Rate

The fundamental process of star formation in the interstellar medium is not yet well known. Phenomenologically, the star formation rate is often represented as a power of the amount of interstellar gas (Schmidt law). The present study follows the result by Kennicutt (1989), who has found from a compilation of data for a number of nearby disk galaxies that the star formation rate per unit area of the galactic disk is proportional to N-th power of the surface density of the gas which includes both molecular and atomic hydrogen. In the present model, this relation is represented as,

$$SFR = \alpha \Sigma_g^N R^2, \tag{4}$$

where Σ_g denotes the gas surface density in the disk and is approximated by $m_g/(\pi R^2)$ in the present multi-component treatment, and α is a coefficient which determines the absolute value of the star formation rate. The range of the power in the above Schmidt law is $N = 1.3 \pm 0.3$ according to Kennicutt (1989). It was found that setting $\alpha = 355 M_\odot yr^{-1}$ produces a range of star formation rate compatible with the observational inference, when the mass, m_g, and the radius, R, are expressed in units of $10^{11} M_\odot$ and 10 kpc, respectively. Therefore α is fixed to $355 M_\odot yr^{-1}$ and N=1, hereafter. Adoption of an universal value of α for all the models is based on the inference that the fundamental star formation process is the same in all the disk galaxies.

The work by Kennicutt (1989) suggests that a certain threshold exists for gas density, below which star formation is effectively inhibited. One plausible interpretation is that the star formation activity is associated closely with the gravitational instability of the gas disk and the threshold corresponds to neutral stability. How is the threshold density determined? One possibility is that the galactic disks have an intrinsic lower limit of velocity dispersion in the gas cloud motion, and a disk with a too small surface density is stabilized by the random motion of the interstellar gas clouds. Indeed, HI and CO observations of nearby galaxies and the Milky Way galaxy suggest near constancy among different galaxies of the velocity dispersion in the atomic and molecular gas clouds (e.g., van der Kruit and Shostak 1984, Stark and Brand 1989). Therefore, I introduced a threshold for star formation by specifying a minimum velocity dispersion which the gas component of the galactic disk can take.

The star formation threshold introduced in the present model works as follows. As explained shortly, the gas disk is assumed to stay at the marginal stability defined by $Q = 1$, where Q denotes the stability parameter introduced by Toomre (1964). At this state, the surface density of the gas and the velocity dispersion (or the sound velocity), σ,

in the gas are related by $\pi G\Sigma_g = \sigma\kappa$, where κ is the epicyclic frequency. As Σ_g decreases in late phase of evolution, σ also decreases correspondingly. However, σ cannot become less than σ_{min}, which is the specified lower limit of the velocity dispersion. Therefore, star formation stops at the instant when σ reaches σ_{min}. The threshold gas surface density is then determined by $\Sigma_{min} = \sigma_{min}\kappa/\pi G$. After this instant, the amount of the gas consumed by star formation is balanced with the amount of the gas added to the disk by accretion, so that the gas surface density is always kept nearly at the threshold value (i.e., $\Sigma_g \sim \Sigma_{min}$). As a special case, setting $\sigma_{min} = 0$ allows star formation to proceed continuously depending on the current gas density.

4.3. Dynamical Friction Timescale

Noguchi (1996) applied the classical Chandrasekhar formula in evaluating τ_{fri}. It is, however, doubtful that this formula, which assumes homogeneous and infinite background of randomly moving light particles, can be safely applied to a heavy body orbiting in a highly flattened and systematically rotating disk component. Quinn & Goodman (1986) have extensively discussed sinking process of satellite galaxies through galactic disks and suggest several analytical evaluations of the orbital decay timescale.

Instead of applying a certain analytical formula, I have resorted to a more empirical approach in evaluation of τ_{fri}. I have run a number of numerical simulations for a massive rigid body (the clump, hereafter) orbiting in the disk plane of a galaxy model, varying the clump mass, the disk surface density, the velocity dispersion of disk stars, and the shape of the rotation curve (see Appendix for numerical details). Time variation of the galactocentric distance of the clump in each model is plotted in Figure 5. Because all the models show a remarkably similar behavior when the time axis is suitably adjusted, I decided to define τ_{fri} as the time it takes the clump to move from the initial radius, $r = 0.8$, to the final radius, $r = 0.2$.

Measurement of τ_{fri} in these experiments is summarized in Table 1. It is evident that the mass of the clump and the surface density of the disk are the key parameters which determine the dynamical friction timescale. Dependence of τ_{fri} on other parameters is weak and can be neglected for the practical range of interest. This is fortunate because little is known in this analytical treatment about the time variation of the disk velocity dispersion or the shape of the rotation curve. Examination of the parameter dependence has led to the following empirical formula for τ_{fri}.

$$\frac{\tau_{fri}}{\tau_{dyn}} = 0.25(\frac{m_{cl}}{M})^{-0.5}(\frac{\Sigma}{M/R^2})^{-0.67}. \quad (5)$$

Here, $\tau_{dyn}[\equiv (GM/R^3)^{-1/2}]$ is the dynamical time of the galaxy, m_{cl} is the mass of the clump, and Σ is the surface density of the total disk which includes both gas and stars, i.e., $\Sigma = (m_g + m_s)/(\pi R^2)$.

In calculating the clump mass, it is assumed that the gas disk is always maintained in the marginally unstable state with Q=1. This assumption finds justification as follows. If $Q > 1$ at a certain moment, no star formation is expected to occur, because the gas disk is stable gravitationally to small scale perturbations. Then Q decreases, because heat input from massive stars is lacking and the gas radiates its energy. When the decreasing Q cuts the value of unity and becomes slightly smaller than unity, the instability sets in and stars begin to form. These stars provide the gas with energy through supernova explosions and stellar winds. Then Q is elevated above unity again. Thus the value of Q will oscillate around $Q = 1$, and $Q = 1$ is a good approximation of the dynamical state of the gas disk.

In the state of marginal instability (or stability), the mass of the clump formed is given by,

$$m_{cl} = \pi(0.5\lambda_c)^2\Sigma_g = \frac{\pi^5\Sigma_g^3}{\kappa^4}, \quad (6)$$

where the critical wavelength $\lambda_c = \frac{2\pi^2\Sigma_g}{\kappa^2}$ and the epicyclic frequency is approximated as $\kappa = (2M/R^3)^{0.5}$. Clump formation is related to star formation closely in the present model. To be consistent with introduction of a star formation threshold, clump formation is inhibited when $\Sigma_g < \Sigma_{min}$. Instantaneous value of τ_{fri} is determined by combining equations (5) and (6). The bulge mass, m_b, thus calculated through equation (3) may be uncertain by a considerable amount because of many simplifications made in the present formulation. However, relative comparison of m_b between different models will be meaningful, and I focus on qualitative behavior of the bulge growth in what follows.

Now equations (1), (2), and (3), combined with auxiliary equations (4), (5), and (6), complete a set of equations which determine the temporal evolution of the system. By integrating these equations numerically starting from the initial condition, $m_g = m_s = m_b = 0$, we know time evolution of any physical quantities of interest.

4.4. Important Parameters: β and Γ

Evolution of a galactic disk in the present formulation is determined mostly by two parameters, the accretion timescale, β, and the mass fraction of the primordial gas, Γ. Before dealing with more complicated cases, I here discuss what effect these parameters have on the disk evolution. Two model series are considered, in order to isolate the effect of varying each parameter. In Series A, only the value of β is changed with all other model parameters being equal, while all the models in Series B have the same parameters but Γ. The mass and the radius of the galaxy are fixed to $M = 10^{11} M_{\odot}$ and $R = 10kpc$ in both series.

Figure 6 shows time evolution of the models in Series A. It is seen that, as β decreases, the peak values of the gas mass fraction (m_g/M), the star formation rate, and the clump mass become larger and are attained at a progressively earlier epoch. On the other hand, the present-day values of the gas mass fraction, the star formation rate, and the clump mass are larger for a model with slower accretion. The bulge formation starts and finishes at an earlier epoch, as β decreases. A smaller β also leads to a larger bulge. The mass of the stellar disk at the present epoch is smaller for a smaller β, because a larger fraction of the accreted material goes to the bulge component in this case, due to more efficient inflow of matter caused by more massive gas clumps. Thus the models in Series A show qualitatively different time evolution depending upon the value of β. It should be noted that the bulge growth caused by the inflow is heavily reduced or stopped when the disk becomes mostly stellar.

What about the effect of varying Γ? Figure 7, which plots temporal behavoir of Series B, indicates that all the models in this family exhibit a qualitatively similar time evolution. Each quantity changes as time in a similar way, and no remarkable effect of varying Γ is observed. Effect of varying Γ manifests only as the difference in the absolute value. Dotted lines in Figure 7 indicate the values divided by Γ of each model. Rough equality in the normalized values of m_s/M, m_g/M, and SFR among different models indicates that these quantities are roughly proportional to the mass fraction, Γ. On the other hand, the normalized clump mass and the normalized bulge mass show a difference of ~ 10 among the calculated models. Thus these quantities behave in a highly nonlinear way with respect to Γ. This strong nonlinearity leads to a large difference in the ratio of the bulge to the disk, or the B/T.

Real galaxies have a large range in both mass and size, so that the two model series discussed above (which assume fixed M and R) are highly idealized. It is inconceivable that two galaxies identical in their mass and size have largely different collapse time β or mass fraction Γ. Likely dependence of β and Γ on the galaxy property should be taken into

account in order to construct more realistic models.

4.5. Collapse Timescale: β

Infall of the gas from outside the disk plane is a natural consequence of galaxy formation from extended halos. It has been also introduced into chemical evolution models to reproduce the metallicity distribution in the solar neighborhood and the age-metallicity relation (e.g., Lacey and Fall 1985).

It is very difficult to deduce quantitatively the time scale of the protogalaxy collapse from observational data. However, several correlations observed among spiral galaxy properties, especially colors and gas contents, provide a circumstantial evidence that this timescale, β, varies from galaxy to galaxy in a systematical way. Late-type disk galaxies have a larger mass fraction of the interstellar medium relative to the galaxy total mass (e.g., Young 1990, Casoli et al. 1998) and bluer total colors (e.g., de Vaucouleurs 1974, Gavazzi 1993) than early-type spirals. These characteristics indicate that the stellar population in late-type galaxies is relatively younger, suggesting a slower build-up of their disks, in view of the results for the model series A discussed above. Although variation along the Hubble sequence appears substantial, dependence on the galaxy luminosity seems to be much larger. The well known color-magnitude relation (e.g., Tully et al. 1982) states that the galaxy becomes bluer as it becomes fainter. Recent analysis by Gavazzi(1993) has found that about two-thirds of the total variation in spiral galaxy color are due to luminosity difference, and only one-third is contributed by the dependence on the Hubble morphological type. The galaxy luminosity has a large influence also on the gas content. Gavazzi's (1993) plots for separate morphological classes show that at a fixed morphological type the relative gas content increases by ~ 10 as the galaxy luminosity decreases by 4-5 magnitudes. Actually, the dependence on the luminosity seems to be stronger than the morphological type dependence, being consistent with large scatter of the gas mass fraction at a fixed morphological type seen in Young (1990).

Systematic change of the collapse timescale along the Hubble type and the galaxy luminosity is plausible also from a theoretical point of view. A spiral galaxy of an earlier morphology tends to have a higher density of matter within its optical extent at the same luminosity as suggested by its larger rotational velocity (e.g., Rubin et al. 1985). It is likely that the collapse timescale is significantly governed by the radiative cooling of the primordial gas in the protogalaxy, and if this is the case, a higher density should have led to a more rapid collapse owing to more efficient cooling. On the other hand, a smaller galaxy may have been more strongly affected by the energy injection from internal star

formation process than a more massive galaxy. Then the collapse of a small galaxy must have been prolonged considerably by the feedback from the initial star formation [Such feedback mechanisms would have caused mass loss from the system or even disintegration of the system in the case of sufficiently intense star formation as expected in dwarf ellipticals, see Yoshii and Arimoto (1987), for example].

These considerations have led to a specification of the collapse timescale as a decreasing function of both the galaxy mass and the internal density. The present model assumes a generalized parameterization of this dependence as follows.

$$\beta = c(\frac{M}{10^{11}M_{\odot}})^{a}(\frac{\rho}{0.1M_{\odot}pc^{-3}})^{b}(Gyr). \tag{7}$$

Here, the density of the galaxy is defined by $\rho = M/R^3$, and c is the coefficient to determine the absolute value of the collapse timescale. The power indices, a and b, determine the steepness of the dependence, and a larger value adopted for each results in a larger range in the collapse time. Both indices are likely to be negative from the discussion above.

A simple consideration suggests that the range in β should be smaller than a factor of ten for the whole population of disk galaxies. First of all, a collapse time smaller than a few times $10^8 yr$ will lead to formation of an elliptical galaxy rather than a spiral, because such a rapid collapse within a few dynamical times of the system will initiate fast star formation which consumes most of the gas before the system reaches a centrifugal equilibrium. A plausible upper limit to the collapse timescale comes from the fact that most disk galaxies appear to have already finished collapse to the disk plane by the present epoch. If the collapse is still continuing, we should see considerable amount of gas at a large distance from the galactic plane, which should be emitting X-ray radiation corresponding to the virial temperature of the galaxy. *ROSAT* observations of neaby spiral galaxies (Read et al. 1997) indicate that the amount of such hot gas outside the galactic plane is less than $\sim 10^9 M_{\odot}$, which is less than 10 percent of the galaxy total mass for S0-Sc galaxies in their sample. This observation, though yet to be extended to a larger sample, seems to preclude a collapse time which is a large fraction of the age of the universe.

To summarize, I considered two cases as follows.

(1) $a = -\frac{1}{2}$, b=0, and c=2.0

(2) $a = -\frac{1}{3}$, $b = -\frac{1}{3}$, and c=2.5

A steeper power of a and a slightly smaller value of c in case (1) have been taken to render the range of β in the considered (ρ, M) domain nearly the same in both cases. As an

additional constraint, an upper limit of 5 Gyr is imposed upon β. Actually, the value of β is likely to depend also on the position in the galaxy (e.g., Matteucci and François 1989, Lacey and Fall 1985, Larson 1976). The value which is used in the present multi-component modeling should be regarded as an averaged value characteristic of the whole galaxy.

4.6. Primordial Gas Fraction: Γ

Another important parameter, Γ, i.e., the fraction of mass which eventually accretes to the galactic plane, is not well constrained from observations, either. It seems to be reasonable to assume that Γ is equal to the combined mass fraction (relative to the total galaxy mass) of the bulge and the disk including interstellar medium, because there is no firm evidence that at the present epoch a significant amount of matter resides in the halo component except dark matter as stated above. Under this assumption, reliable determination of Γ is still hampered. One ambiguity arises from our poor knowledge about the mass-to-luminosity ratio for the luminous components. This ratio depends strongly on the formation history (i.e., time variation of the star formation rate) and the initiall mass function of the stellar population considered, which are generally difficult to deduce. On the other hand, the total mass, M, seems to be well determined from the rotation curve at least for non-barred galaxies, for which the circular rotation provides a fairly exact description of the disk kinematics.

Comparing the empirical relation between the mass-to-luminosity ratio, M/L_B, and the $B-V$ color of spirals with the theoretical one predicted by Larson & Tinsley's (1978) photometric evolution model, Tinsley (1981) found that the observed increase of M/L_B with the $B-V$ is much shallower than that theoretically predicted, suggesting that late-type spirals have relatively more dark matter than early-type ones. Thus, Tinsley (1981) has claimed that the halo mass fraction is the dominant parameter controlling the morphological type. Athanassoula et al. (1987) also find that the dominance of the dark matter is larger in bluer galaxies. However, Jablonka & Arimoto (1992) have recently concluded that the halo mass ratio is universal among spiral galaxies (at least from Sa to Sc), based on a detailed population synthesis analysis treating the bulge and the disk separately. Also, decomposition models for a selected sample of spirals having well measured rotation curves seem to show no systematic variation of this ratio along the Hubble sequence (e.g., van der Kruit and Searle 1982, Bahcall and Casertano 1985).

Persic & Salucci (1988), on the other hand, conclude that the dark-to-luminous mass ratio within the optical radius increases as the galaxy becomes less luminous. According to the result by Ashman (1990) which is based on Persic & Salucci (1988), a galaxy with

a mass of $10^{10}M_{\odot}$, for example, has a twice larger mass fraction of the dark matter on average compared with the most massive galaxies, although the dispersion at a fixed mass is considerably large [see Fig.2 of Ashman (1990)].

In view of these arguments, I considered three cases as follows.

(1) $\Gamma = 0.12logM - 1.00$

(2) $\Gamma = 0.15logM + 0.15log\rho - 2.56$

(3) $\Gamma = 0.50$

4.7. Model Families

I have calculated two families of models, differing in the star formation process. In one family, star formation is allowed to take place always depending on the gas density by taking $\sigma_{min} = 0$. These models are called continuous models. A finite threshold, $\sigma_{min} = 3(kms^{-1})$, was specified in another group (hereafter, threshold models). Each calculated model is specified by three parameters as (c or t)-(β type)-(Γ type), where "c" and "t" denotes continuous and threshold specification for star formation, respectively, and types for β and Γ denote the corresponding specifications given in §4.5 and §4.6, respectively. For example, t-1-3 means the model in which β is a function only of the mass, Γ is constant, and the star formation threshold is introduced. All the possible combinations of the three parameters have been computed, leading to 12 models in total. In each model, the galaxy evolution has been calculated at (8×8) grid points on the (ρ, M) plane, which are equally spaced both in $log\rho$ and in $logM$. The ranges of mass and density are $10^{10}M_{\odot} \leq M \leq 3 \times 10^{12}M_{\odot}$, and $6 \times 10^{-3}M_{\odot}pc^{-3} \leq \rho \leq 1M_{\odot}pc^{-3}$, respectively. The star formation coefficient was fixed to $\alpha = 355M_{\odot}yr^{-1}$.

In the followings, the results of these models are confronted with the currently available observational data.

5. Observational Material

Before detailed examination of the model results, this section summarizes the observational data with which the models are compared. I confine comparison to the "classical" spirals, i.e., to the morphological type from Sa to Sc. The observational data, especially those for the bulge-to-disk luminosity ratio, are well accumulated only for this range of morphology.

5.1. Bulge-to-Disk Ratio

Several studies have tried to measure the luminosity ratio of the bulge and disk components by the decomposition technique (e.g., Yoshizawa and Wakamatsu 1975, Kent 1985, Simien and de Vaucouleurs 1986). Figure 8 shows the observed bulge-to-total luminosity ratio as a function of galaxy mass and density, for the sample used by Whitmore (1984), which is itself based on the observations by Rubin, Ford, and Thonnard (1980) and Rubin et al. (1982). I calculated the mass and density for the sample galaxies from the optical radius (i.e., the radius at which the surface brightness in B-band is 25 mag arcsec^{-2}), R_{25}, and the rotational velocity, V_{25}, at the optical radius as

$$M = GR_{25}V_{25}^2$$

and

$$\rho = MR_{25}^{-3},$$

where G is the gravitational constant. Both R_{25} and V_{25} have been taken from Rubin et al. (1980, 1982). The mass thus calculated will give an approximately correct value for the optical part of the galaxy, but the density calculated here should be regarded as a rough characteristic value for that galaxy, because of a steep density gradient inside the galaxy.

It is recognized in Figure 8 that, on the average, the B/T increases as the galaxy mass increases at a fixed galaxy density, and at a fixed galaxy mass it increases with the density. However, it is difficult to represent the bulge-to-total luminosity ratio as a function of one single parameter. The principal component analysis carried out by Whitmore (1984) indicates that the surface brightness of the galaxy is only one physical quantity (among parameters he investigated) which shows significant correlation with the B/T. Indeed, the lines of constant surface mass density plotted in Figure 8 run roughly in parallel with loci of constant B/T, although the irregularity in the distribution of the B/T is large. In order to see the observed tendency more clearly, Figure 9 divides the whole sample into two subgroups according to mass or density, and plots the B/T against the galaxy mass or the density, separately for each subgroup. The significance level, P, is given, at which the null hypothesis of zero correlation is disproved as well as the correlation coefficient, r. The correlation is confirmed with a confidence level of > 95 percent in all cases. Another compilation by Dale et al. (1997) also supports the dependence of the B/T on the galaxy mass and the galaxy density displayed in Figure 8. They do not give the B/T but only the Hubble type for the sample galaxies. Figure 10 shows the Hubble morphological type

distribution on the (ρ, M)-plane for the Dale et al. (1997) sample. It is clear that a more massive or denser galaxy tends to have an earlier morphological type, and that the regions occupied by galaxies with the same Hubble morphological type are also elongated in similar directions to the constant surface density lines.

The observed values of the B/T should be taken with caution. The measurement of the bulge-to-disk luminosity ratio is a very delicate task. Usually a light distribution model composed of a de Vaucouleurs' bulge (i.e., the $r^{1/4}$-law) and an exponential disk is fitted to the observed surface brightness profile. However, this method is criticized recently (e.g., Andredakis and Sanders 1994, de Jong 1996) on the ground that the de Vaucouleurs' density distribution does not decrease sufficiently fast as the radius so that the fitting is significantly influenced by the irregular light distribution sometimes observed at larger radii. Andredakis & Sanders (1994) propose exponential form for both the bulge and the disk for better decomposition. The result by de Jong (1996) using this method shows a clear trend that the B/T decreases as the morphological type becomes later both in B and K bands, as expected. The scatter around the mean relation is large, however. Also the measured B/T with an exponential bulge is systematically smaller than the one obtained by the de Vaucouleurs' model by a factor of 3-5. It should also be noted that any decomposition technique works best when the contributions from the bulge and the disk are comparable. On the other hand, detection of a faint disk in the presence of a luminous bulge or a small bulge embedded in a bright disk is difficult.

5.2. Gas Content and Star Formation Rate

Although the primary aim of the present study is to understand the formation of galactic bulges, any successful model of galaxy evolution should be able to explain the observed trend in the gas content and the star formation activity among galaxies of different type and luminosity.

Young (1990) shows that the mass ratio of the gas including both neutral and molecular hydrogens relative to the dynamical mass calculated from the rotation curve decreases systematically as the morphological type becomes earlier. The gas fraction given by Young (1990) ranges from 0.03 for Sa-Sab galaxies to 0.3 for Scd galaxies. The scatter within the same morphological type is as large as ~ 10, however. The ratio of molecular to neutral hydrogens decreases as the Hubble type becomes later. Gavazzi (1993) provides extensive data for HI content in disk galaxies. His data show that HI flux per unit H flux increases as the morphological type becomes later as expected. At a fixed type, HI/H is an increasing function of the H-band luminosity of the galaxy, indicating that less massive galaxies are

more gas-rich on the average.

I take here two samples by Young et al. (1989) and Sage (1993), which are given in a convenient form for plotting on the (ρ, M) plane. Figure 11 plots the mass fraction of the gas by Young et al. (1989). From their original sample of 182 galaxies, I deleted those galaxies which lack mass estimate for either HI or H_2. Those galaxies suspected to be in ongoing interactions/mergers or in abnormal star formation activity (e.g., Markarian galaxies) have also been deleted. For the remainder, the ratio of the total gas mass to the galaxy mass within the optical radius has been calculated and plotted on the (ρ, M) plane. A global trend is recognized in this figure that the gas mass ratio increases as the galaxy mass increases or the galaxy density decreases, though the scatter in the ratio is considerably large. This systematic variation is even clearer for the sample by Sage (1993), which is plotted in Figure 12. The gas fraction is seen to increase monotonically toward the lower-left corner of the diagram. Quantitative evaluation of the gas mass fraction needs caution, especially for molecular hydrogens. The conversion factor from the observed CO luminosity to H_2 mass is not known accurately, and may be different from galaxy to galaxy depending on the metallicity. Another ambiguity comes from the fact that the neutral hydrogen generally extends much farther than the optical radius. The procedure taken here tends to overestimate the gas mass ratio within the optical radius.

The largest set of star formation rate measurements is given by Kennicutt (1983), who calculated the SFR for a number of spiral galaxies from H_α luminosity. Figure 13 plots the SFR measured by him on the (ρ, M) plane. Only an upper limit of the SFR is given for most Sa galaxies. The distribution pattern of the SFR is not easy to grasp.

However, the plot of the normalized star formation rate, i.e., SFR/M, on this plane reveals a clear trend (Fig.14). The galaxies with higher SFR/M values occupy a lower region in the (ρ, M) plane. This is qualitatively consistent with the known luminosity effect that the gas fraction increases and the color becomes bluer as the galaxy becomes fainter. However, there appears to be no clear trend from Kennicutt's (1983) data that the normalized SFR increases for less dense (hence correspondingly later on average) galaxies. This seems to be at odds with the behavior of the gas fraction plotted in Figures 11 and 12, which suggests a stronger dependence of the gas content on the galaxy density than on the galaxy mass. This may be due partly to heavy obscuration of H_α emission by dust, which should be more severe in late-type spirals. These somewhat puzzling results indicate a necessity for more improved and extensive observational data.

5.3. Epoch of Bulge Formation

When and how rapid the galactic bulges have been formed is one of the most important but unsolved problems regarding disk galaxies. For example, the age of the Milky Way bulge and the age spread in the bulge stars have not yet been tied down to sufficient accuracy (e.g., Matteucci and Brocato 1990, Holtzman et al. 1993, Rich 1996, Norris 1996). Although quantitative assessment is difficult, it is possible that the age of the bulge is different from galaxy to galaxy. Metallicity observations by Jablonka et al. (1996) show that the value [Mg/Fe] decreases as the bulge becomes fainter. This may indicate that a smaller bulge possessed in general by galaxies of later morphological types (see Fig.1 of Jablonka et al. 1996) has been formed in a more extended period, though a definite answer should wait accurate models of chemical evolution.

Peletier and Balcells (1996) have recently found that the optical and near-infrared colors of the bulge are very similar to those of the disk in a number of spiral galaxies of type S0 to Sbc; A blue bulge is likely to be associated with a blue disk. One possible interpretation is that the age of the bulge is correlated with that of the disk and the age difference is a small portion of the age of the universe. At the same time, their data seem to suggest a large difference in the bulge age among different galaxies. Fitting of single age, single metallicity stellar population models by Vazdekis et al. (1996) to the $U - R$ and $R - K$ colors of the observed bulges suggests that a number of bulges can have ages as young as 4 Gyr and a few bulges may have even younger ages of ~ 1 Gyr. Nevertheless, reliable age determination for old stellar populations is difficult because of degeneracy of their colors.

Recent imaging observations of the nearby galaxy bulges carried out by Carollo et al. (1997) with the HST/WFPC2 provide intriguing results. They found that a considerable percentage of the observed bulges exhibit irregular morphology, being composed of a few discrete clumps. Carollo et al. (1997) infer that the bulge formation is not a completed process associated with the initial protogalactic collapse, but may be still ongoing or has been finished only recently in some galaxies. They propose a disk origin for the bulge matter, and invoke bar structures as a tool driving an inflow of disk matter to the galactic center. The observation by Carollo et al. (1997) suggests that the irregular bulges are more frequent in spiral galaxies of later morphological types (see their Fig.3), and this may indicate later and/or more prolonged formation of the bulge in a galaxy of a later type.

6. Model Results

This section describes the model results and attempts comparison with the observational data. The variation of the collapse timescale, β, and the primordial gas fraction, Γ, is shown in Figure 15. Comparison is carried out by using the (ρ, M) plane. It is permitted in fitting the models to the observations to slide the ρ-axis and/or the M-axis by a small amount. Because the present analytical model treats only *characteristic* values of the galaxy, there is some ambiguity about galaxy mass and density. Especially, the density is a poorly defined quantity because of its steep variation with the galactocentric radius. Furthermore, even if the galaxy density is defined to be an average density within the optical radius (i.e., R_{25} usually), a discrepancy of this radius between different authors (because of different Hubble constants adopted, for example) would be much exaggerated in evaluation of the density, through inverse cubic dependence of the density on the radius. These ambiguities should be kept in mind whenever the models are compared with the observations.

6.1. Bulge-to-Disk Ratio

All of the twelve calculated models exhibit a variation of the bulge-to-disk ratio as a function of galaxy mass and density, which is qualitatively consistent with the observation. Figure 16 plots the mass ratio of the bulge relative to the total luminous matter, $B/T \equiv m_b/(m_b + m_s)$, for all the models calculated. Comparison of these values with the observed B/T luminosity ratios should be done carefully. The difference in the mass-to-luminosity ratio in bulges and disks will not totally justify equating the mass ratio to the luminosity ratio. Also the observed luminosity ratio depends on the decomposition technique used (§5.1). Thus I pay attention primarily to qualitative behavior of the B/T ratio. The calculated B/T increases as the density and/or the mass of the galaxy increases, showing the qualitatively same behavior as the observation suggests. It is encouraging that the range in the B/T plotted in Figure 16 is roughly equal to the observed range given by de Jong's (1996) K-band photometry for galaxies from Sa to Sc. Although the slopes of B/T contours depend on the adopted specification of β and Γ, the comparison with Figure 8 does not favor any particular model nor reject it.

One intriguing effect of the star formation threshold, common to all the threshold models calculated, is an increase of the bulge-to-disk ratio for least massive galaxies, for which all the continuous models give smallest B/T ratios. This curious behavior is caused by substantial amount of the interstellar gas unused by star formation in these low density galaxies. This phenomenon may be important in understanding of evolutionary status of extremely late galaxies, and will be discussed in the forthcoming paper.

Figure 17 plots the B/T against β. Correlation between the two quantities is not always tight. Modulation by the galaxy density or the mass fraction, Γ, is not neglected in general. Therefore, the conclusion by Noguchi (1998) that the bulge-to-disk ratio is determined primarily by the collapse timescale (i.e., the disk formation timescale) is not supported. The previous conclusion was derived from more limited calculations in which both the galaxy mass and the galaxy density are fixed and only the collapse timescale was varied (such as Series A in §4.4), and may be errorneous. Nevertheless, it is true that the accretion timescale has a strong influence on the resulting bulge-to-disk ratio.

6.2. Present Gas Content and Star Formation Rate

Figure 18 displays the mass fraction of the gas component, m_g/M, at the present epoch. In continuous models, the collapse timescale β governs the gas consumption rate strongly, so that the present gas fraction is tightly correlated with β. Thus the continuous models with β dependung only on the galaxy mass (c-1-1, c-1-2, and c-1-3) exhibit nearly horizontal contours of m_g/M in the (ρ, M) plane. This behavior may contradict with the observations by Young et al. (1989) and Sage (1993), which suggest much steeper contours (see Figures 11 and 12). On the other hand, the continuous models with β being a decreasing function of both mass and density (c-2-1, c-2-2, and c-2-3) seem to reproduce the observed trend at least qualitatively.

One possible problem with these continuous models is that the absolute value of the gas mass fraction tends to be considerably smaller than observed, as much as by a factor of ~ 10. This discrepancy may not rule out these models convincingly, however. There is a substantial discrepancy between the interstellar gas masses determined by different authors. For example, Casoli et al. (1998) give the gas fraction of $\sim 5 \times 10^{-3}$ for Sa galaxies to $\sim 2 \times 10^{-2}$ for Sc galaxies, which is considerably smaller than the values by Young(1990) and is in better agreement with the models.

Introduction of a threshold gas density controlled by a constant minimum velocity dispersion of the gas disk improves the result remarkably. In this case, the gas content at the present epoch is determined solely by the galaxy parameters, M and ρ (through the epicyclic frequency), and does not depend on the star formation history of the galaxy. This is because the galaxy, in the considered (ρ, M) domain, has already reached to the infall-limited regime of star formation by the present epoch. The gas mass fraction as a function of M and ρ is the same in all the threshold models, and increases as M and/or ρ decreases, in qualitative agreement with the observation. It is seen that inhibition of star formation by the threshold boosts up the present-day gas content, and brings the models

into a better agreement with the observational data. The observations by Kennicutt (1989) also suggest that the interstellar gas in many spiral galaxies is in the infall-limited regime at present.

The specific star formation rate, SFR/M, in the continuous models follows the same behavior as the gas fraction on the (ρ, M) plane (Fig.19). Regarding star formation, the continuous models with β depending only on the galaxy mass (c-1-1, c-1-2, and c-1-3) seem to be in best agreement with the observation by Kennicutt (1983) plotted in Figure 14, though these models may contradict the observation of the gas content as stated.

The threshold models show sporadic starbursts when the gas density is nearly equal to the threshold density. This makes the contours of SFR/M at the present epoch very irregular on the (ρ, M) plane. Comparison with the observation is not straightforward. Although the model galaxy exhibits starbursts, it is premature to conclude that the galaxy really experiences a burst. A real galaxy will be described as a sum of a number of local regions, over each of which coherence of evolution is maintained. The present multi-zone model treats one particular region as the representative one and traces its time evolution. In other words, this modelling does not take into account existence of many local regions which evolve more or less independently. In real galaxies, random behavior (or phase difference) of individual regions will smear out starbursts taking place in local regions, and a global starburst will not be realized unless evolution of many regions is cynchronized by some mechanism.

6.3. Formation Epoch of Bulges

Figure 20 indicates the epoch of bulge formation, t_{bulge}. Here t_{bulge} is defined to be the epoch at which half the final bulge mass has been accumulated. The bulge formation epoch in all the calculated models becomes earlier as the mass and/or the density of the galaxy increases. The B/T ratio is anticorrelated with the formation epoch roughly, which may agree with the observed decrease of the [Mg/Fe] ratio as the bulge becomes fainter (Jablonka et al. 1996) and the preponderance of irregular bulges in late-type spirals (Carollo et al. 1997). A good positive correlation is found between t_{bulge} and β. Because β also determines the major epoch of disk formation, this correlation may explain the similarity in colors between the bulge and the disk in many spiral galaxies observed by Peletier and Balcells (1996).

The age of the bulge indicated in Figure 19 may be argued to be too large, especially for less massive and/or less dense galaxies. The present multi-zone model cannot make

allowance for the likely variation of the collapse timescale at different radii in the galaxy. The value of β should be regarded as a kind of average over the entire disk, and tends to overestimate the actual accretion timescale in the inner disk, which contributes to the bulge formation much. This limitation presumably leads to an overestimate of t_{bulge}. Anyway, measured age difference between the bulge and the disk in a galaxy will depend strongly on how extended part of the disk is considered, because of a large difference of the accretion timescale at different radii in the disk component.

7. Discussion

It has been demonstrated that the clumpy evolution model can reproduce the observed variation of the bulge-to-disk ratio among spiral galaxies for a wide range of possibility which will encompass the real situation. Nevertheless, the quality of the available observational data and the limitation in the theoretical modelling seem to hamper further narrowing of the parameter range. Here I discuss a few implications of the present study and limitations of the models.

7.1. Appearance of Primeval Disk Galaxies

Only few studies have explored what primeval galaxies might really look like (e.g., Meier 1976, Baron and White 1987, Katz 1992). Theoretical predictions on appearance of young galaxies are becoming increasingly important, because direct observations of high-redshift galaxies enabled by HST and other new instruments start to provide powerful constraints on theoretical evolutionary models from morphological and dynamical viewpoints.

The CDM cosmogony predicts clumpy appearance of primeval galaxies as a direct consequence of dominant small-scale density perturbations imposed on the matter distribution in the early universe. Indeed, Baron and White (1987) demonstrate by numerical simulations that a young *elliptical* galaxy should not be observed as a bright single body but as a conglomeration of several discrete blobs connected by a common faint envelope. Katz's(1992) dissipational formation model for a spiral galaxy, including star formation process, also produces clumpy appearance at high redshift, because of imposed initial density perturbations. In this case, the clumps form during the collapse of the galaxy.

In contrast to these CDM-based simulations, the clumps advocated in the present study have no causal relationship with initial density perturbations in the universe. The clumpy nature of primeval disk galaxies in the present model originates in the gravitational

instability of gas-rich galactic disks formed in the early phase of disk galaxy evolution. It is encouraging that HST and large ground-based telescopes have recently found clumpy structures in a number of high-redshift galaxies, although they may be manifestation of CDM clumps. The number of clumps contained in one object is a few usually, though this number may be severely affected by the spatial resolution and the surface brightness limit of the instrument used. Even chain galaxies (e.g., Cowie et al. 1995), which are elongated objects containing several bright blobs, may be primeval disk galaxies viewed edge-on, in which the clumps scattered in the disk component are viewed within the projected disk plane [Another possibility is suggested by Dalcanton and Shectman (1996) that they represent edge-on low surface brightness galaxies]. Head-tail systems called "tadpole" galaxies by van den Bergh et al.(1996) may not be a rectilinear object but edge-on manifestation of a clumpy disk in which one of several clumps is particularly large.

Another possible evidence for clumpy structures other than from direct imaging comes from the analysis of correlation functions. Infante et al. (1996) found, for galaxies with the average redshift of $< z > \sim 0.35$, a discontinuity of the correlation function at the separation of ~ 6 arcsec. This suggests strong clustering of faint galaxies within ~ 20 kpc of individual galaxies, which may be caused by clumping in a single galactic disk. Because the mean redshift of their sample is relatively small, it is desirable to extend similar analysis into a larger redshift.

One caveat in interpreting images of distant galaxies is that morphology of objects at large redshift is strongly influenced by k-correction and the steep dependence of surface brightness on redshift (of the form $(1+z)^{-5}$). Bohlin et al. (1991) and Giavalisco et al. (1996a) have cautioned that those clumpy structures observed in medium to high redshift galaxies may not be the features characteristic of early evolution phases but simply be an exaggerated manifestation of the irregular distributions of star forming regions such as observed in some galaxies (usually of late types) in the local universe.

Interactions or mergers with smaller satellite galaxies are sometimes invoked in the interpretation of peculiar appearance of high redshift galaxies (e.g., Griffiths et al. 1994, van den Bergh et al. 1996). The most straightforward and powerful test to discriminate between the instability hypothesis proposed here and the merger/interaction scenario is to examine the kinematics of "satellites". In the merger/interaction scenario, we expect random orientation of clump orbits relative to the primary because there is no reason to consider that the bombardment of other galaxies from outside has any preferred geometry with respect to the primary. On the other hand, it is inevitable in the present scenario that the motions of "satellites" are co-planar and all the satellites rotate in the same direction around a common center. Spectroscopic observations will provide a direct check.

7.2. Creation of the Bulge-Disk Structure

The traditional Hubble classification scheme is based on three morphological characteristics; prominence of the bulge relative to the disk, the pitch angle of the spiral arms, and the degree of resolution of the arms into stars (Sandage 1961). However, Sandage et al. (1970) argue that the most fundamental parameter distinguishing between different Hubble types is the relative gas content, presumed to have been determined at the time of formation. Yoshizawa & Wakamatsu (1975) found that the relative prominence of the disk and bulge components is well correlated with the morphological type, and argue that disk galaxies are specified quantitatively by both the bulge-to-disk ratio (as a morphological indicator) and the luminosity of the disk (as a scale indicator). Van den Bergh (1976) has proposed a two-dimensional classification scheme in which the bulge-to-disk ratio and the gas content are independent parameters, with the former determined by the formation process while the latter changeable due to environmental factors. These propositions are, however, made on more-or-less phenomenological grounds and do not always address in what manner these fundamental quantities (such as the gas content and the bulge-to-disk ratio) have been determined in the evolution of a particular galaxy. More systematic and quantitative attempts include application of the principal component analysis to determine the number of independent parameters defining galaxies. Brosche (1973) and other groups have concluded that just two dimensions could explain most of the observed diversity in spiral galaxies.

Dynamical study of the formation and evolution process of galaxies has a long history (e.g., Eggen et al. 1962). One of the most important goals in this area is to understand origins of the observed variety of galaxies. A series of numerical works carried out by Larson (1969, 1974, 1975, 1976) stand out as a landmark in the theoretical galactic astronomy. In his models, the formation of a disk galaxy proceeds in two stages characterized by star formation processes that operate at very different rates. First, there is a rapid star formation process that forms a spheroidal component, and later a much slower star formation permits most of the residual gas to condense into a disk before it is consumed by star formation. Larson (1976) envisages two possibilities as the cause of the reduction of the star formation efficiency after the bulge formed, which is required for the formation of a significant disk component. The first is inhibition of star formation by the tidal force exerted on the gas clouds by the already existing bulge. Second possibility is that the protogalactic gas has a two-phase structure with dense clouds that rapidly form stars in a spheroidal component and less dense intercloud gas which does not form stars until it has settled to a disk. He has also prescribed turbulent viscosity which is large in the early phase of evolution when the bulge grows but is reduced in later phases, in order to get distinct separation between the disk and the bulge. Using these settings, Larson (1976) has reached to the conclusion

that the bulge-to-disk ratio depends mostly on the star formation rate, which is in turn controlled by the initial density or velocity dispersions in protogalaxies.

In marked contrast with Larson's (1976) model, the present study proposes a more disordered and chaotic formation of disk galaxies. The dominance of massive subgalactic clumps and resulting dynamical processes constitute the main ingredient of the present model. The bulge is assembled from those clumps formed by the local gravitational instability in the disk component. The model appears not to require two star formation processes operating at different timescales, unlike the models constructed by Larson (1976), though more realistic simulations would be necessary to establish this point. In the present model, the clumpy nature of the young gas-rich disk provides the required viscosity to form a bulge (e.g., Lin and Pringle 1987). Larson (1976) had to introduce viscosity *a priori* because the axisymmetry of the configuration imposed on his models could not allow radial transport of angular momentum by non-axisymmetric perturbations such as clumps, bars, and spiral arms. Although the present study stresses the secondary nature of the galactic bulges, this does not mean that the *whole* disk has formed before the bulge, as repeatedly cautioned. Only inner parts of the disk contribute to bulge formation, and outer parts are considered to form much later than the bulge by a slow accretion of the primordial gas from the outer halo. In this respect, the present scenario is not so drastically different from Larson's (1976) model as it might seem.

7.3. Longevity of Clumps

The present study stresses the importance of heavy clumps formed in the early galactic disks in driving long-term disk galaxy evolution. Therefore the longevity of these clumps is a key factor of the present model. Although the present study takes into account the contribution from the formed clumps of all the mass scales, it may be considered that clumps with smaller masses are prone to destruction in general. The possible destruction processes include energy injection from internal star formation and tidal destruction due to the galaxy gravitational field. Strong concentration of the gas clouds into narrow spiral arms observed in nearby galaxies points to relatively short lifetimes for those clouds. For example, the giant molecular clouds , with masses of $\sim 10^6 M_\odot$, are considered to have a lifetime shorter than a few times $10^8 yr$, perhaps due to energy deposit from young massive stars born in them. Even giant molecular associations (GMAs), with estimated masses of several times $10^7 M_\odot$, seem to be transient. Rand & Kulkarni (1990) found that GMAs in the inter-arm regions of M51 are gravitationally unbound, and argued that they may be disrupting due to tidal shearing by the background gravitational field of the galaxy. If this

is correct, the estimated lifetime of these GMAs is several times 10^8 yr. The present model sometimes develops clumps with masses of $10^{8-9} M_\odot$. Fate of these extremely massive clumps is not clear because they are absent from nearby (i.e., present-day) galaxies. Such clumps may also suffer from disintegration.

Then is the treatment in the present study totally unrealistic? Answer is probably 'No'. Assuming that a clump of any mass has a finite lifetime, probably depending on its internal structure and the strength of the external tidal field, the interstellar gas in real galaxies will be circulated through different phases as follows. First , a group of clumps will be formed owing to gravitational instability in the gas disk. Untill these clumps are destroyed by some mechanism, they will feel dynamical frictions and move inward to the galactic center. When the clumps are destroyed, clump material is dispersed into the interstellar space and the inflow driven by dynamical friction stops. However, after a certain period, a new generation of clumps are formed from this diffuse material by gravitational instability, and they resume inward motion. Actually, this recycling will not be a coherent process over the entire galactic disk, but every local region in the disk will experience recycling with its own phase, independently of each other.

The numerical simulation described in §2 and §3 differs from the situation considered here despite that it does include energy feedback from star formation events in a simple form. The massive clumps formed in the numerical model maintain their identity untill they merge with other clumps or they are swallowed by the bulge. On the other hand, the analytical multi-component models presented in §4 seem to better fit in with the circulation picture of the interstellar medium. They calculate the typical mass of clumps from the instantaneous gas surface density. Therefore, the clump mass is changing as a function of time. In other words, the models do not assume the identity of each clump for the whole period of galaxy evolution. Then, those analytic models provide a fairly good description of actual situation, provided that the average lifetime of clumps is a significant fraction of the whoel period of one circulation cycle.

7.4. Undiscussed Issues

The present study has mainly discussed a limited range of the whole family of spiral galaxies, namely, from type Sa to Sc. These galaxies occupy the upper right half of the (ρ, M) plane employed here. Compared with these galaxies, relatively little is known about galaxies later than Sc, which occupy the lower left part of the (ρ, M) diagram. The present study may provide an interesting implication for these galaxies as stated in §6.1, but it will be treated in a separate paper.

Another issue which may be related to the problem of extremely late galaxies is the evolutionary status of the low surface brightness galaxies. Recent observations have been providing a mounting evidence that the realm of galaxies is actually dominated by very faint galaxies which have eluded past observations. The universality of the disk central surface brightness (Freeman 1970) is turning out to be due to selection effect, and those galaxies with a central brightness fainter than $\sim 23B$ mag arcsec^{-2}, which are often called low surface brightness (LSB) galaxies (Impey and Bothun 1997 and references therein), may occupy as much as half the total galaxy population. LSB galaxies tend to be of a late morphological type (Schombert et al. 1992), though early-type analogues are sometimes observed (Sprayberry et al. 1995). One possibility is that most LSB galaxies represent a continuation of disk galaxies into morphological types later than Sd and Sm. Protogalactic systems with a high angular momentum and/or a low mass are suggested to be precursors of LSB galaxies (Dalcanton et al. 1997). Global characteristics of LSB galaxies have been investigated intensively in recent years (e.g., de Blok et al. 1995, de Blok et al. 1996, de Blok and McGaugh 1997). Most LSB galaxies appear to lack any significant bulge component. However, interestingly enough, Sprayberry et al. (1995) report several giant LSB galaxies possessing a large bulge component.

It is not clear at present how these LSB galaxies can be incorporated into the galaxy evolution model proposed here. Since the present model is a model of bulge formation largely, more detailed information on the bulge-to-disk ratio for LSB galaxies is necessary to examine whether the present model can accomodate the class of LSB galaxies as its part or not.

8. Conclusions

Collapse of a protogalaxy composed of dark matter and primordial gas has been investigated by numerical simulations and analytical multi-zone modelling in an attempt to examine early evolution of disk galaxies. Importance of the ample interstellar matter existing in young galactic disks has been highlighted. Confrontation of the theoretical results with the available observational data has led to a new picture for disk galaxy evolution, in which the bulge is the secondary object formed from disk matter.

As the protogalaxy collapses, a gaseous disk starts to form. Very few stars form before the disk formation because the gas density is low. The formation of the disk causes drastic increase in the gas density and initiates star formation process. The galactic disk in early evolution phases is rich in the interstellar gas and the efficient energy dissipation keeps the disk dynamically cold. Then the gravitational instability sets in, leading to the formation

of massive clumps rotating in the disk plane. The individual mass of these clumps can be as large as $\sim 10^9 M_\odot$. Intense star formation occurs in these clumps. Therefore, the galaxy at this epoch exhibits a clumpy and irregular appearance in optical wavelengths, which may give explanation of morphologically peculiar galaxies observed at high redshift. While orbiting in the disk plane, the clumps tend to merge with each other and make successively larger clumps. The clumps loose their orbital kinetic energy through dynamical friction against surrounding stars and gas clouds, and accumulate to the central region, thus forming a spheroidal bulge. The collapse timescale of the protogalaxy will be larger in its outer parts. Slower accretion of the primordial gas is considered to have established outer parts of the disk after the bulge formation is mostly finished.

Simple analytical models have been constructed, in which a disk galaxy is described as a multi-component system comprising a dark halo, gaseous and stellar disks, and a bulge. Evolution of these components is controlled by two parameters; the accretion timescale, i.e., the rapidness with which the primordial gas contained in the halo region accretes to the disk plane, and the mass fraction of the primordial gas at the beginning. Based on the observational evidence, the accretion timescale in real spiral galaxies has been assumed to be a decreasing function of both the galaxy mass and the galaxy density, whereas the fraction of the primordial gas has been assumed to increase as the galaxy mass and/or the galaxy density increases. Under this specification, the analytical modelling of the clumpy galaxy evolution picture has succeeded in reproducing the observational result that a galaxy having a large total mass and/or a large internal density tends to have a large bulge-to-disk ratio, which is established at least for the morphology range of Sa to Sc. This success suggests importance of the clumpy evolution in young disk galaxies, though the evolution of real spiral galaxies may be a more complicated process comprising several fundamentally different mechanisms.

NUMERICAL EVALUATION OF SINKING TIMESCALE OF A CLUMP

A massive body orbiting in the disk component of a galaxy spirals in to the galactic center by the action of dynamical friction. The timescale of this inward motion of the clump has been evaluated by numerical simulations as follows. Parameters of each simulation are listed in Table 1.

N-body models for a disk galaxy, which consists of a halo and a disk, have been constructed first. The models contain no interstellar gas. Here, the halo is not meant to represent the entire (dark) halo which might surround the visible galaxy, but the portion of the dark halo *inside* the optical radius plus any luminous spheroidal components such as a bulge. The total mass of the galaxy is unity and the mass of the disk component is m_d. Both components are truncated at the galactocentric radius of unity. The halo and the disk are constructed by 5000 and 50000 collisionless particles, respectively. The gravitational softening radius is 0.04 and 0.02 for the halo and disk particles, respectively.

The model is fundamentally based on Fall & Efstathiou (1980). The stellar disk has an exponential surface density distribution with a scale length of 0.25, in agreement with observations. The disk rotates nearly rigidly in the inner parts and at a nearly constant velocity in the outer parts. The turn-over radius which divides these two parts is denoted by r_m. Thus the global shape of the rotation curve is determined by specifying r_m. The halo is assumed to be spherically symmetric, and its volume density distribution is determined so that the rotational velocity in the disk plane due to the combined gravitational field of the halo and the disk matches the specified rotation curve.

The velocity dispersion of the halo is chosen as follows. First, the isotropic velocity dispersion at each radius is calculated so that the condition for "local virial equilibrium" is satisfied everywhere (see Noguchi 1991 for details). A trial simulation showed that such a condition does not lead to virial equilibrium for the entire system. In order to alleviate this, the velocity dispersion was multiplied by a factor of 0.65.

This disk galaxy model is evolved in isolation before the sinking simulations. First only the halo component is evolved for 15 dynamical times with the disk component fixed. After the halo is relaxed, the disk is activated. At this time, the gravitational force acting on each disk particle is calculated and the circular velocity is given to that particle so that the centrifugal force is exactly balanced with the gravity. Next, small random velocities are given to disk particles , which correspond to a specified Q parameter of Toomre (1964). The rotational velocity of each star is then corrected for the contribution from this random motion. This state just after the activation of the disk is adopted as the initial condition for the disk galaxy in the sinking simulations.

The clump is treated as a particle which has a mass, m_{cl}, and a gravitational softening radius of r_s, which is regarded as the effective radius of the clump. The mass and radius of the clump given in Table 1 are also in units of those of the disk galaxy. The clump starts at the galactocentric radius $r = 0.8$ in the disk plane. The initial velocity is that of the circular motion, and the orbital motion is in the same direction as the disk rotation. This initial condition is appropriate for the clumps formed from the disk material. A number of simulations have been carried out by varying m_d, m_{cl}, r_m, and Q. Each simulation is performed untill the galactocentric radius of the clump decreases to 0.2. Epoch of this moment is taken to be the dynamical friction timescale, τ_{fri}, and listed in Table 1. Gravitational interactions between all the particles have been calculated by the tree code (e.g., Barnes and Hut 1986), and the orbit integration has been done by the leap-frog scheme with a time step of 0.01, i.e., one hundredth of the dynamical timescale (A time step of 0.015 was used in the halo relaxation phase).

Table 1. Timescale of dynamical-friction induced sinking.

Model	m_d	m_{cl}	r_m	Q	τ_{fri}[a]	note[b]
1	0.3	0.01	0.3	1.5	5.41	
2	0.1	0.01	0.3	1.5	11.4	
3	0.2	0.01	0.3	1.5	7.32	
4	0.3	0.03	0.3	1.5	3.78	
5	0.3	0.003	0.3	1.5	11.1	
6	0.3	0.001	0.3	1.5	21.7	r_s=0.02
7	0.3	0.01	0.1	1.5	5.31	
8	0.3	0.01	0.7	1.5	6.32	
9	0.3	0.01	0.3	1.0	5.29	
10	0.3	0.01	0.3	2.0	5.96	
11	0.3	0.01	0.3	1.5	4.75	r_s=0.02
12	0.3	0.01	0.3	1.5	4.92	r_s=0.04

[a]The timescale, τ_{fri}, is the time it takes the clump to move from $r = 0.8$ to $r = 0.2$, and its unit is the dynamical time of the galaxy.

[b]The effective radius of the clump, r_s, is 0.07 unless specified.

REFERENCES

Abraham, R.G., Tanvir, N.R., Santiago, B.X., Ellis, R.S., Glazebrook, K., and van den Bergh, S. 1996, MNRAS, 279, L47

Andredakis, Y.C., and Sanders, R.H. 1994, MNRAS, 267, 283

Ashman, K.M. 1990, ApJ, 359, 15

Athanassoula, E., Bosma, A., and Papaioannou, S. 1987, A&A, 179, 23

Bahcall, J.N., and Casertano, S. 1985, ApJ, 293, L7

Barnes,J.E., and Hut,P. 1986, Nature, 324, 446

Baron, E., and White, S.D.M. 1987, ApJ, 322, 585

Bohlin, R.C. et al. 1991, ApJ, 368, 12

Brosche, P. 1973, A&A, 23, 259

Carollo, C.M., Stiavelli, M., de Zeeuw, P.T., and Mack, J. 1997, AJ, 114, 2366

Casoli, F. et al. 1998, A&A, 331, 451

Cole, S., Aragon-Salamanca, A., Frenck, C.S., Navarro, J.F., and Zepf, S.E. 1994, MNRAS, 271, 781

Cowie, L.L., Hu, E.M., and Songaila, A. 1995, AJ, 110, 1576

Dalcanton, J.J., and Shectman, S.A. 1996, ApJ, 465, L9

Dalcanton, J.J., Spergel, D.N., and Summers, F.J. 1997, ApJ, 482, 659

Dale, D.A., Giovanelli, R., Haynes, M.P., Scodeggio, M., Hardy, E., and Campusano, L.E. 1997, AJ, 114, 455

de Blok, W.J.G., van der Hulst, J.M., and Bothun, G.D. 1995, MNRAS, 274,235

de Blok, W.J.G., McGaugh, S.S., and van der Hulst, J.M. 1996, MNRAS, 283, 18

de Blok, W.J.G., and McGaugh, S.S. 1997, MNRAS, 290, 533

de Jong, R.S. 1996, A&A, 313, 45

de Vaucouleurs, G. 1974, in IAU Symp. 58, The Formation and Dynamics of Galaxies, ed. J.R. Shakeshaft (Dordrecht: D.Reidel Publishing Company), 1

de Vaucouleurs, G., de Vaucouleurs, A., Corwin, H.G., Jr., Buta, R.J., Paturel, G., and Fouqué, P. 1991, Third Reference Catalogue of Bright Galaxies (New York: Springer-Verlag) (RC3)

Driver, S.P., Windhorst, R.A., and Griffiths, R.E. 1995, ApJ, 453, 48

Ebisuzaki, T., Makino, J., Fukushige, T., Sugimoto, D., Ito, T., and Okumura, S.K. 1993, PASJ, 45, 269

Eggen, O.J., Lynden-Bell, D., and Sandage, A.R. 1962, ApJ, 136, 748

Fall, S.M., and Efstathiou, G. 1980, MNRAS, 193, 189

Fall, S.M., and Rees, M.J. 1985, ApJ, 298, 18

Freeman, K.C. 1970, ApJ, 160, 811

Gavazzi, G. 1993, ApJ, 419, 469

Giavalisco, M., Livio, M., Bohlin, R.C., Macchetto, F.D., and Stecher, T.P. 1996a, AJ, 112, 369

Giavalisco, M., Steidel, C.C., and Macchetto, F.D. 1996b, ApJ, 470, 189

Glazebrook, K., Ellis, R., Santiago, B., and Griffiths, R. 1995, MNRAS, 275, L19

Glazebrook, K., Lehár, J., Ellis, R., Aragón-Salamanca, A., and Griffiths, R. 1994, MNRAS, 270, L63

Gott, J.R., and Thuan, T.X. 1976, ApJ, 204, 649

Griffiths, R.E. et al. 1994, ApJ, 435, L19

Hausman.,M.A., and Roberts,W.W. 1984, ApJ, 282,106

Henriksen, R.N. 1991, ApJ, 377, 500

Holtzman, J.A. et al. 1993, AJ, 106, 1826

Impey, C., and Bothun, G. 1991, ARA&A, 35, 267

Infante, L., de Mello, D.F., and Menanteau, F. 1996, ApJ, 469, L85

Jablonka, P., and Arimoto, N. 1992, A&A, 255, 63

Jablonka, P., Martin, P., and Arimoto, N. 1996, AJ, 112, 1415

Katz, N. 1992, ApJ, 391, 502

Katz, N., and Gunn, J.E. 1991, ApJ, 377, 365

Kennicutt, R.C. 1983, ApJ, 272, 54

Kennicutt, R.C. 1989, ApJ, 344, 685

Kent, S.M. 1985, ApJS, 59, 115

Koo, D.C. et al. 1996, ApJ, 469, 535

Kormendy, J. 1993, in IAU Symp. 153, Galactic Bulges, eds. H. Dejonghe and H.J. Habing (Dordrecht: Kluwer Academic Publishers), 209

Lacey, C.G., and Fall, S.M. 1985, ApJ, 290, 154

Larson, R.B. 1969, MNRAS, 145, 405

Larson, R.B. 1974, MNRAS, 166, 585

Larson, R.B. 1975, MNRAS, 173, 671

Larson, R.B. 1976, MNRAS, 176, 31

Larson, R.B., and Tinsley, B.M. 1978, ApJ, 219, 46

Levinson,F.H., and Roberts,W.W. 1981, ApJ, 245,465

Lin, D.N.C., and Pringle, J.E. 1987, MNRAS, 225, 607

Matteucci, F., and François, P. 1989, MNRAS, 239, 885

Matteucci, F., and Brocato, E. 1990, ApJ, 365, 539

McWilliam, A., and Rich, R.M. 1994, ApJS, 91, 749

Meier, D.L. 1976, ApJ, 207, 343

Navarro, J.F., and White, S.D.M. 1994, MNRAS, 267, 401

Noguchi, M. 1991, MNRAS, 251, 360

Noguchi, M. 1996, ApJ, 469, 605

Noguchi, M. 1998, Nature, 392, 253

Norris, J.E. 1996, in IAU Symp. 169, Unsolved Problems of the Milky Way, ed. L.Blitz and P.Teuben (Dordrecht: Kluwer Academic Publishers), 353

Peletier, R.F., and Balcells, M. 1996, AJ, 111, 2238

Persic, M., and Salucci, P. 1988, MNRAS, 234, 131

Quinn, P.J., and Goodman, J. 1986, ApJ, 309, 472

Rand, R.J., and Kulkarni, S. 1990, ApJ, 349, L43

Read, A.M., Ponman, T.J., and Strickland, D.K. 1997, MNRAS, 286, 626

Rich, R.M. 1996, in IAU Symp. 169, Unsolved Problems of the Milky Way, ed. L.Blitz and P.Teuben (Dordrecht: Kluwer Academic Publishers), 403

Roberts,W.W., and Hausman,M.A. 1984, ApJ, 277,744

Rubin, V.C., Ford, W.K.,Jr., and Thonnard, N. 1980, ApJ, 238, 471

Rubin, V.C., Ford, W.K.,Jr., Thonnard, N., and Burstein, D. 1982, ApJ, 261, 439

Rubin, V.C., Burstein, D., Ford, W.K., Thonnard, N. 1985, ApJ, 289, 81

Sage, L.J. 1993, A&A, 272, 123

Sandage, A. 1961, The Hubble Atlas of Galaxies (Washington, D.C., Carnegie Institution of Washington)

Sandage, A. 1986, A&A, 161, 89

Sandage, A.R., Freeman, K.C., and Stokes, N.R. 1970, ApJ, 160, 831

Schombert, J.M., Bothun, G.D., Schneider, S.E., and McGaugh, S.S. 1992, AJ, 103, 1107

Shlosman, I., and Noguchi, M. 1993, ApJ, 414, 474

Simien, F., and de Vaucouleurs, G. 1986, ApJ, 302, 564

Solomon, P.M., Sanders, D.B., and Scoville, N.Z. 1979, in IAU Symp. 84, The Large-Scale Characteristics of the Galaxy, ed. W.B.Burton (Dordrecht: Reidel), 35

Sprayberry, D., Impey, C.D., Bothun, G.D., and Irwin, M.J. 1995, AJ, 109, 558

Stark, A.A., and Brand, J. 1989, ApJ, 339, 763

Steidel, C.C. 1990, ApJS, 74, 37

Steidel, C.C., Giavalisco, M., Dickinson, M., and Adelberger, K.L. 1996a, AJ, 112, 352

Steidel, C.C., Giavalisco, M., Pettini, M., Dickinson, M., and Adelberger, K.L. 1996b, ApJ, 462, L17

Steinmetz, M., and Müller, E. 1995, MNRAS, 276, 549

Tinsley, B.M. 1981, MNRAS, 194, 63

Tóth, G., and Ostriker, J.P. 1992, ApJ, 389, 5

Toomre, A. 1964, ApJ, 139, 1217

Tully, R.B., Mould, J.R., and Aaronson, M. 1982, ApJ, 257, 527

van den Bergh, S. 1976, ApJ, 206, 883

van den Bergh, S., Abraham, R.G., Ellis, R.S., Tanvir, N.R., Santiago, B.X., and Glazebrook, K.G. 1996, AJ, 112, 359

van der Kruit, P.C., and Searle, L. 1982, A&A, 110, 61

van der Kruit, P.C., and Shostak, G.S. 1984, A&A, 134, 258

Vazdekis, A., Casuso, E., Peletier, R.F., and Beckman, J.E. 1996, ApJS, 106, 307

Whitmore, B.C. 1984, ApJ, 278, 61

Yoshii, Y., and Arimoto, N. 1987, A&A, 188, 13

Yoshizawa, M., and Wakamatsu, K. 1975, A&A, 44, 363

Young, J.S. 1990, in The Interstellar Medium in Galaxies, eds. H.A.Thronson, & J.M.Shull (Dordrecht: Kluwer Academic Publishers), 67

Young, J.S., Xie, S., Kenney, J.D.P., and Rice, W.L. 1989, ApJS, 70, 699

Fig. 1.— Morphological evolution of the numerical model. (a) The projection of the gas cloud particles onto the x-y plane (i.e., the disk plane). Only half the particles selected at random are displayed. Time, t, in units of Gyr is indicated in the upper right corner of each frame. Coordinates are given in units of kpc. (b) The same as (a) but the projection onto the x-z plane. The x-y and x-z projections of all the stellar particles younger than 10^7 yr are given in (c) and (d), respectively. The stars older than 10^7 yr are displayed in (e) and (f). In panel (e), the five massive clumps used for subsequent alanyses are indicated at t=0.64 Gyr, enclosed by circles.

Fig. 2.— The mass fractions of the gaseous and total disks with respect to the total mass in the numerical model (solid lines). The fraction of the gaseous disk, f_g, is a summation over the gas particles with $|z - z_c| < 0.1R$ and $0.3R < r < 1.5R$, where z_c denotes the z-coordinate of the mean disk plane at each time and r is the cylindrical radius measured from the z-axis. The mass fraction of the total disk, f_d, is the sum of f_g and the mass fraction of the stellar disk. The latter is summed over all the stellar particles with $0.3R < r < 1.5R$. The left panel indicates the evolutionary track on the $f_d - f_g$ diagram, whereas the time evolution of f_g is shown in the right panel. Time, t, is given in units of Gyr here. The dashed lines indicate the evolution of an analytical multi-component model explained in §4. The analytical model plotted here has the same mass and radius as the numerical model. The fraction of the primordial gas is also the same as in the numerical model (i.e., $\Gamma = 0.5$), and the collapse timescale was set to $\beta = 0.3$ Gyr. The dynamical friction timescale given in eq(5) of the text was multiplied by 0.3 in this model. Open circles in the right panel indicate the expected mass of the individual clumps (in units of $M_\odot$) in the analytical model, which is evaluated as explained in §4.3.

Fig. 3.— Time evolution of the star formation rate in the numerical model (solid line). Time, t, and the star formation rate are given in units of Gyr and $M_\odot yr^{-1}$, respectively. The dashed line indicates the SFR in the analytical model plotted in Figure 2.

Fig. 4.— Distribution of the age for the stars contained in the bulge region in the numerical model. The center of the bugle is defined to be that of the most massive clump. Each histogram shows, for the given epoch, the relative number of the stars which were born at the time indicated in the abscissa. Solid lines are distributions for stars located within 0.1 R of the bulge center, whereas the dotted lines for stars located within 0.025 R. Time is in units of Gyr.

Fig. 5.— Sinking of a heavy clump through the stellar disk of model spiral galaxies. Details

of the numerical calculation are given in Appendix. The ordinate indicates the galactocentric distance of the clump in units of the radius of the model galactic disk. The abscissa is the time normalized by the dynamical friction timescale, τ_{fri}, namely the time which takes the clump to move from its initial radius of 0.8 to the final radius of 0.2. Model parameters are given in Table 1., but individual models are not discriminated in this plot.

Fig. 6.— Time evolution of the models in Series A. All the models have the same mass, $M = 10^{11} M_{\odot}$, and the same radius, $R = 10$kpc. Only the accretion timescale, β, has been varied. From the most rapidly increasing curve, $\beta = 0.5$, 1.08, 2.32, and 5.0 Gyr, in all the panels. All the models have Γ=0.5. The dynamical friction timescale given in eq(5) of the text was multiplied by 0.3 in all the models. The star formation rate, SFR, and the mass of the clump, m_{cl}, are in units of $M_{\odot} yr^{-1}$ and $M_{\odot}$, respectively. The mass ratio of the bulge to the total luminous matter, B/T, is defined by $m_b/(m_b + m_s)$.

Fig. 7.— Same as Figure 6 but for the models in Series B, in which only Γ is varied. Four models are indicated here, with Γ=0.1, 0.17, 0.29, and 0.5, from the thinnest to progressively thicker solid curves. All the models have β=2 Gyr. The dynamical friction timescale given in eq(5) of the text was multiplied by 0.3 in all the models. The dashed line indicates, for each model, the quantity divided by Γ of that model. Again, Γ increases as the line becomes thicker. For these normalized quantities, the ordinate is arbitrary, to facilitate only relative comparison between different models. Note that the normalization makes time variation in the masses of the stellar and gaseous disks (m_s, m_g) and the star formation rate (SFR) almost identical in different models, indicating that these three quantities are scaled just in proportion to the mass fraction, Γ, of the initial primordial gas. On the other hand, the clump mass (m_{cl}) and the bulge mass (m_b) show strongly nonlinear dependence on Γ, which leads to largely different final values of B/T.

Fig. 8.— The bulge-to-total luminosity ratios for a sample of spiral galaxies with morphological type of Sa to Sc, taken from Whitmore (1984). The ordinate indicates the mass, M, of the galaxy inside the optical radius in units of $M_{\odot}$, whereas the abscissa indicates the density, ρ, within the optical radius in units of $M_{\odot} pc^{-3}$. The area of each circle is proportional to the B/T ratio for the corresponding galaxy. The dashed lines specify the constancy of the surface density defined by $\Sigma \equiv M/R^2$, where the mass, M, is in units of $M_{\odot}$, and the optical radius, R, is in units of parsec.

Fig. 9.— Correlation of the bulge-to-total luminosity ratio (B/T) and the mass or the density for Whitmore (1984) galaxies plotted in Figure 8. The whole sample is divided into two groups according to the mass or the density, and correlation is examined between the B/T and the other quantity in each subsample. The correlation coefficient, r, and the

probability for the null hypothesis of zero correlation, P, are indicated.

Fig. 10.— Distribution of galaxies with different morphological types on the (ρ, M) plane. The galaxy sample is taken from Dale et al. (1997). The ordinate indicates the mass, M, of the galaxy inside the optical radius in units of $M_\odot$, whereas the abscissa indicates the density, ρ, within the optical radius in units of $M_\odot pc^{-3}$. The dashed lines specify the constancy of the surface density defined by $\Sigma \equiv M/R^2$, where the mass, M, is in units of $M_\odot$, and the optical radius, R, is in units of parsec.

Fig. 11.— Mass fraction of the interstellar gas realtive to the total matter inside the optical radius of the galaxy. The galaxy sample is taken from Young et al. (1989). The ordinate indicates the mass, M, of the galaxy inside the optical radius in units of $M_\odot$, whereas the abscissa indicates the density, ρ, within the optical radius in units of $M_\odot pc^{-3}$. Here the interstellar gas means the sum of the molecular gas and the atomic gas. The area of the circle is proportional to the gas mass fraction. Dotted circles mean upper limits in either molecular mass or atomic mass.

Fig. 12.— Same as Figure 11, but for the sample by Sage (1993). Dotted circles mean upper limits in molecular mass.

Fig. 13.— Star formation rate for the sample of spiral galaxies compiled by Kennicutt (1983). Only galaxies with type Sa to Sc are plotted. The ordinate indicates the mass, M, of the galaxy inside the optical radius in units of $M_\odot$, whereas the abscissa indicates the density, ρ, within the optical radius in units of $M_\odot pc^{-3}$. The data used to calculate the mass and the density are taken from RC3 (de Vaucouleurs et al. 1991). Crosses, which correspond to Sa galaxies mostly, mean non detection of measurable star formation activity. Breakdown of the whole sample by the SFR (in units of $M_\odot yr^{-1}$) is given in other five panels.

Fig. 14.— Same as Figure 13, but for the specific star formation rate, SFR/M, for the sample of spiral galaxies compiled by Kennicutt (1983). Only galaxies with type Sa to Sc are plotted. Here, the specific SFR is defined to be the star formation rate divided by the galaxy mass, M, inside the optical radius, and its unit is yr^{-1}. Crosses, which correspond to Sa galaxies mostly, mean non detection of measurable star formation activity.

Fig. 15.— The accretion timescale, β, and the mass fraction of the primordial gas, Γ, in the analytical multi-zone models. The model name (see text for explanation) is indicated in the upper right corner of each panel. The ordinate indicates the mass, M, of the galaxy inside the optical radius in units of $M_\odot$, whereas the abscissa indicates the density, ρ, within the optical radius in units of $M_\odot pc^{-3}$. The dotted contours correspond to β=1, 2, 3, 4, and 5 Gyr, from the thinnest to progressively thicker lines in all the panels. The solid contours

correspond to Γ= 0.25, 0.3, 0.35, 0.4, and 0.45, from the thinnest to progressively thicker lines in all the panels.

Fig. 16.— Same as Figure 15, but for the ratio of the bulge mass to the total luminous mass at the present epoch, defined by $B/T = m_b/(m_b + m_s)$, where m_b and m_s are masses of the bulge and the disk, respectively. The contours are for log(B/T)=-0.5, -0.75, -1.0, -1.25, and -1.5, from the thickest to progressively thinner lines in all the panels.

Fig. 17.— The bulge-to-luminous mass ratio, B/T, plotted against the accretion timescale, β (in Gyr), for each model.

Fig. 18.— Same as Figure 15, but for the ratio of the gas mass to the total galaxy mass, m_g/M, at the present epoch. The contours are for m_g/M=0.001, 0.002, 0.004, 0.008, 0.016, 0.032, and 0.064, from the thinnest to progressively thicker lines in all the panels.

Fig. 19.— Same as Figure 15, but for the ratio of the star formation rate to the total galaxy mass, SFR/M, at the present epoch. The contours are for SFR/M= (0.5, 1, 2, 4, 8, 16, 32, 64)$\times 10^{-12} yr^{-1}$, from the thinnest to progressively thicker lines in all the panels.

Fig. 20.— Same as Figure 15, but for the epoch of bulge formation, t_{bulge}, which is defined to be the epoch where the bulge mass reached to half of the present value. The contours are for t_{bulge}= 1, 2, 3, 4, and 6 Gyr, from the thinnest to progressively thicker lines in all the panels.

This figure "f1a.gif" is available in "gif" format from:

http://arXiv.org/ps/astro-ph/9806355v1

This figure "f1b.gif" is available in "gif" format from:

http://arXiv.org/ps/astro-ph/9806355v1

This figure "f1c.gif" is available in "gif" format from:

http://arXiv.org/ps/astro-ph/9806355v1

This figure "f1d.gif" is available in "gif" format from:

http://arXiv.org/ps/astro-ph/9806355v1

This figure "f1e.gif" is available in "gif" format from:

http://arXiv.org/ps/astro-ph/9806355v1

This figure "f1f.gif" is available in "gif" format from:

http://arXiv.org/ps/astro-ph/9806355v1

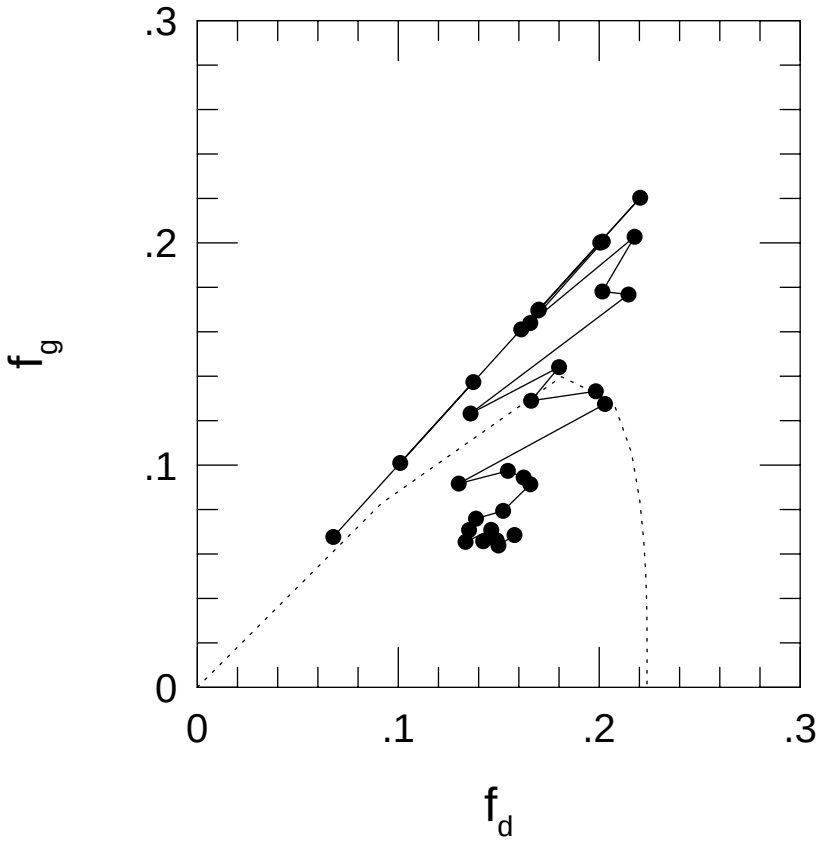
.3
.2
.1
0
0
.1
.2
.3
f_g
f_d

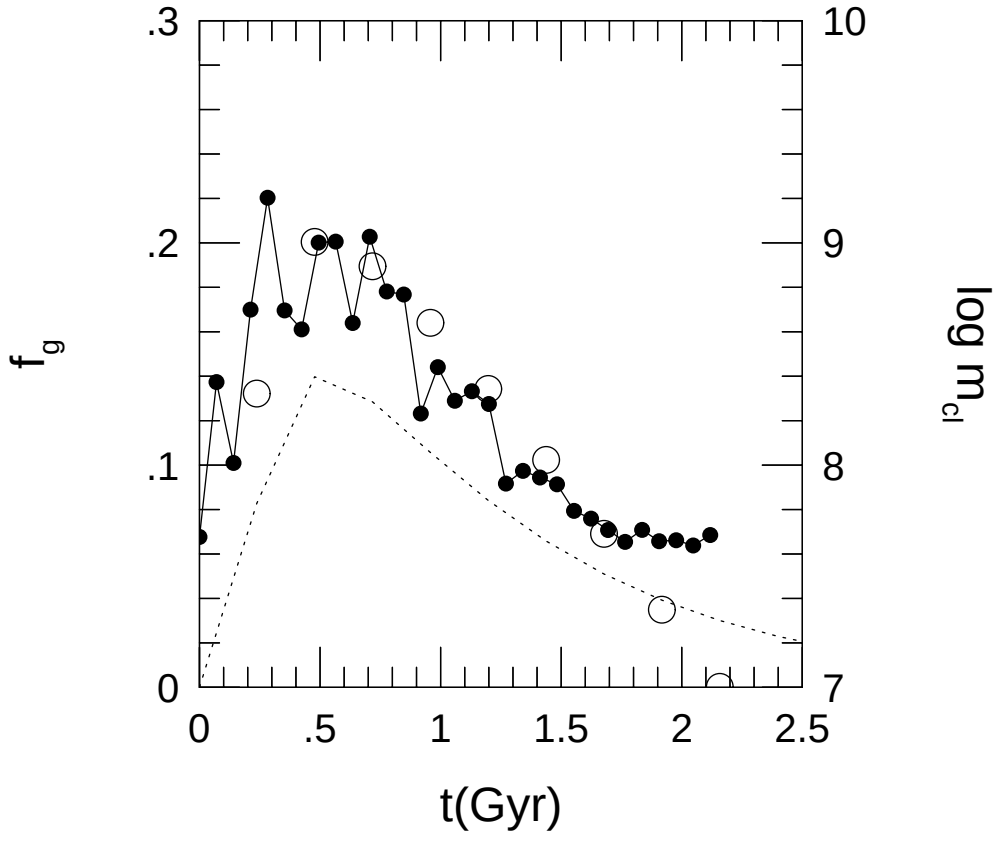
.3
.2
.1
0
0
.5
1
1.5
2
2.5
10
9
8
7
f_g
t(Gyr)
log m_{cl}

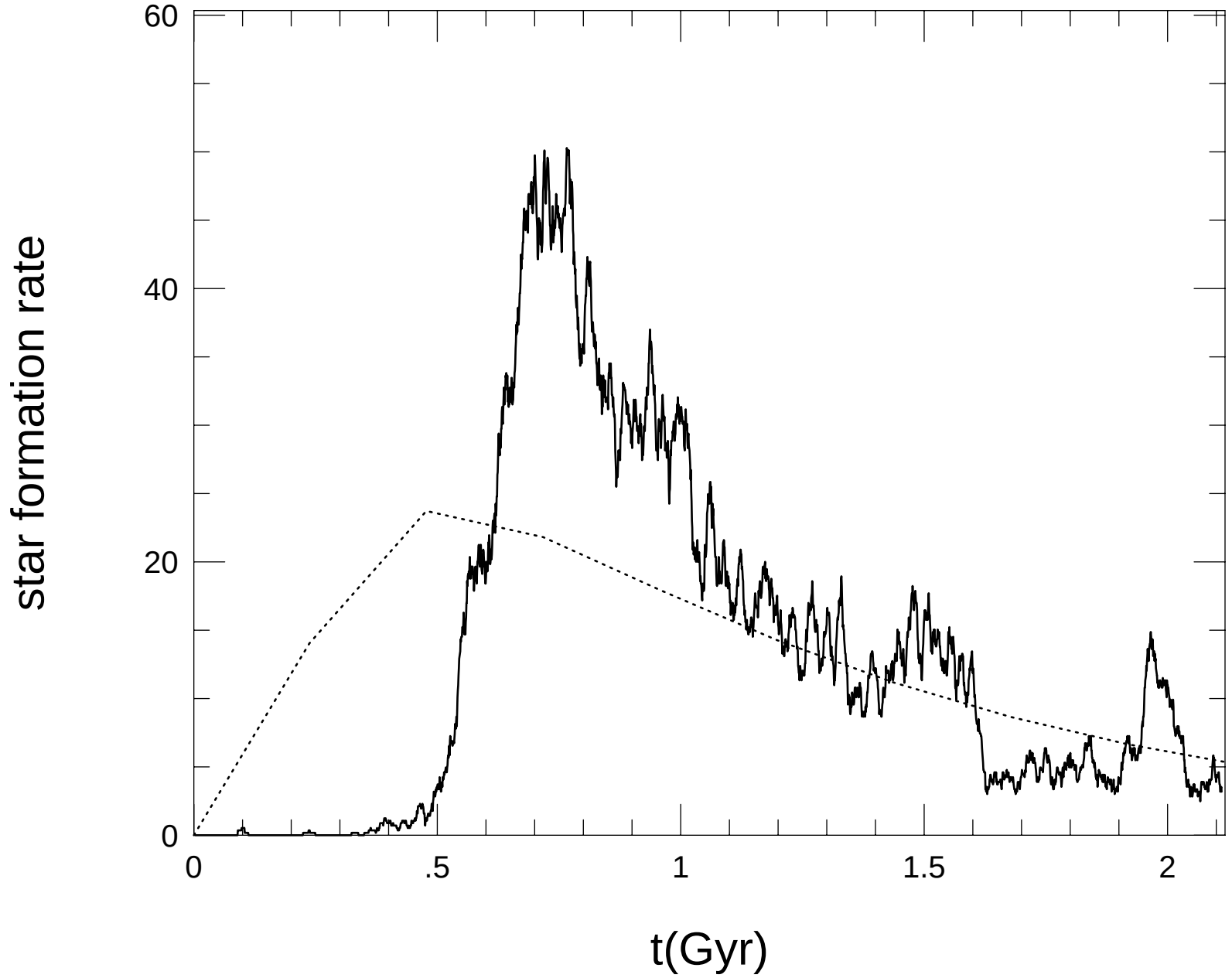
60
40
20
0
0
.5
1
1.5
2
star formation rate
t(Gyr)

Age Distribution in Bulge

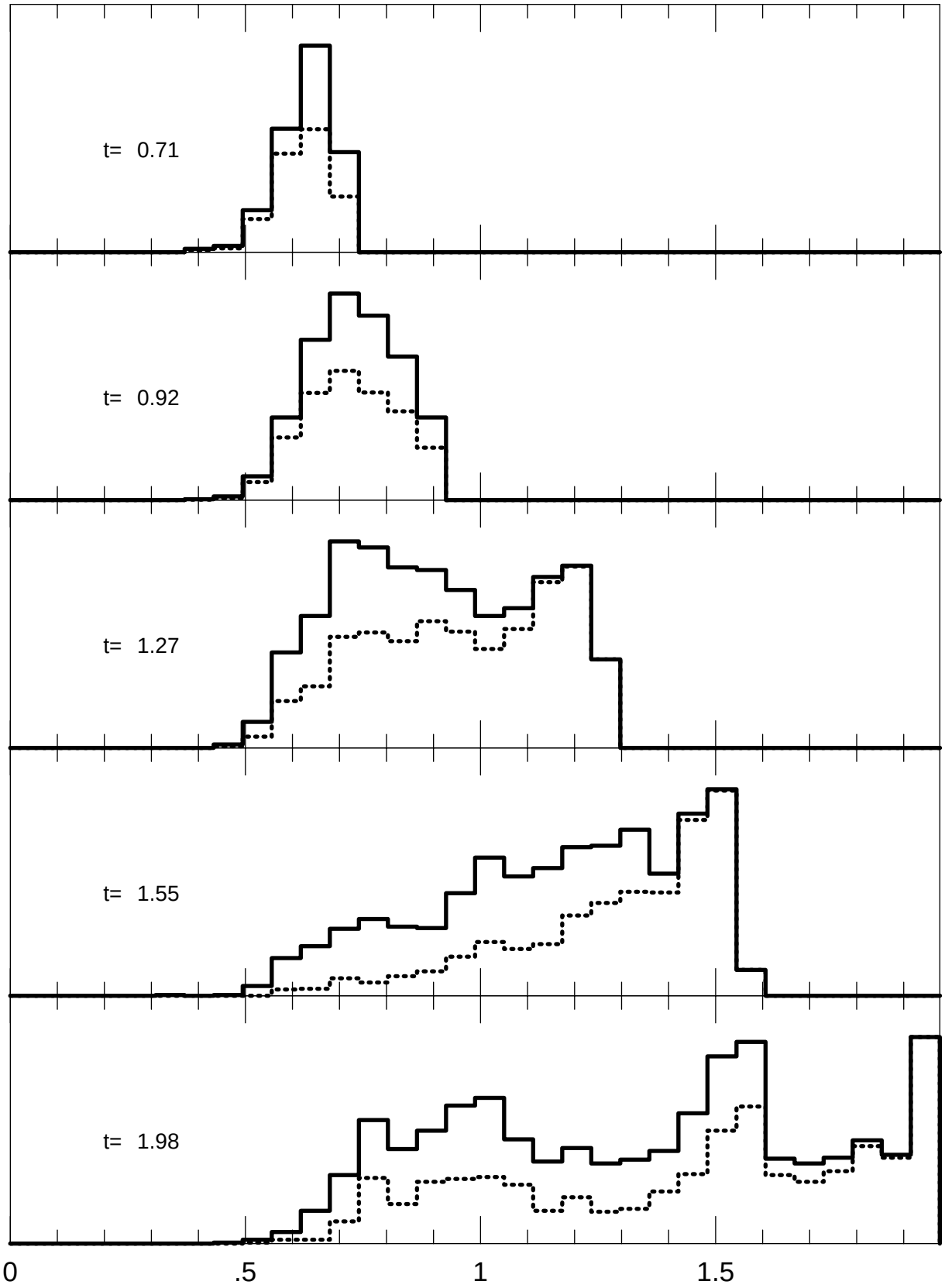

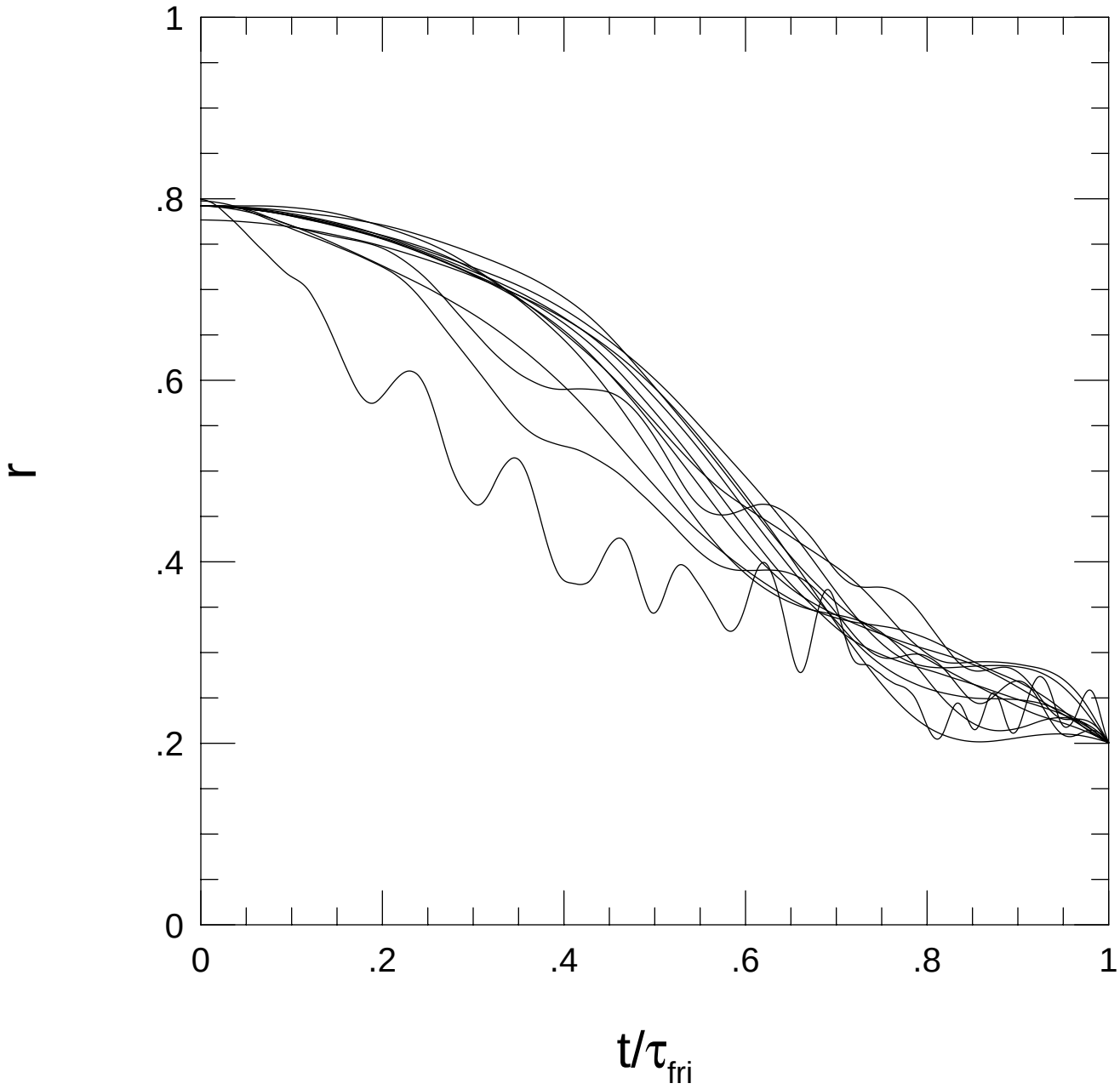
1
.8
.6
.4
.2
0
r
0
.2
.4
.6
.8
1
t/τfri

β-Sequence

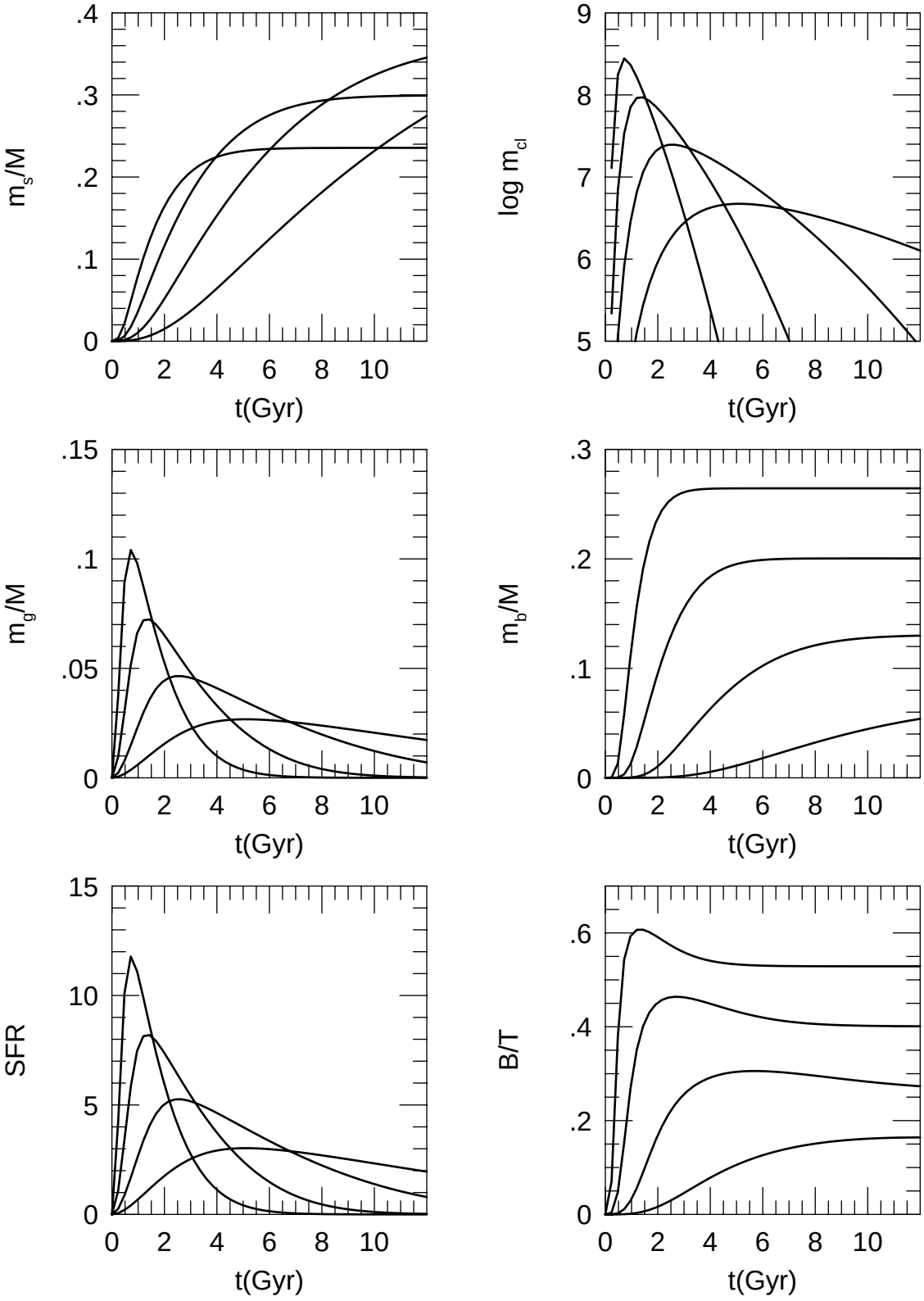
.4
.3
.2
.1
0
m_s/M
0 2 4 6 8 10
t(Gyr)
9
8
7
6
5
log m_{cl}
0 2 4 6 8 10
t(Gyr)
.15
.1
.05
0
m_g/M
0 2 4 6 8 10
t(Gyr)
.3
.2
.1
0
m_b/M
0 2 4 6 8 10
t(Gyr)
15
10
5
0
SFR
0 2 4 6 8 10
t(Gyr)
.6
.4
.2
0
B/T
0 2 4 6 8 10
t(Gyr)

Γ-Sequence

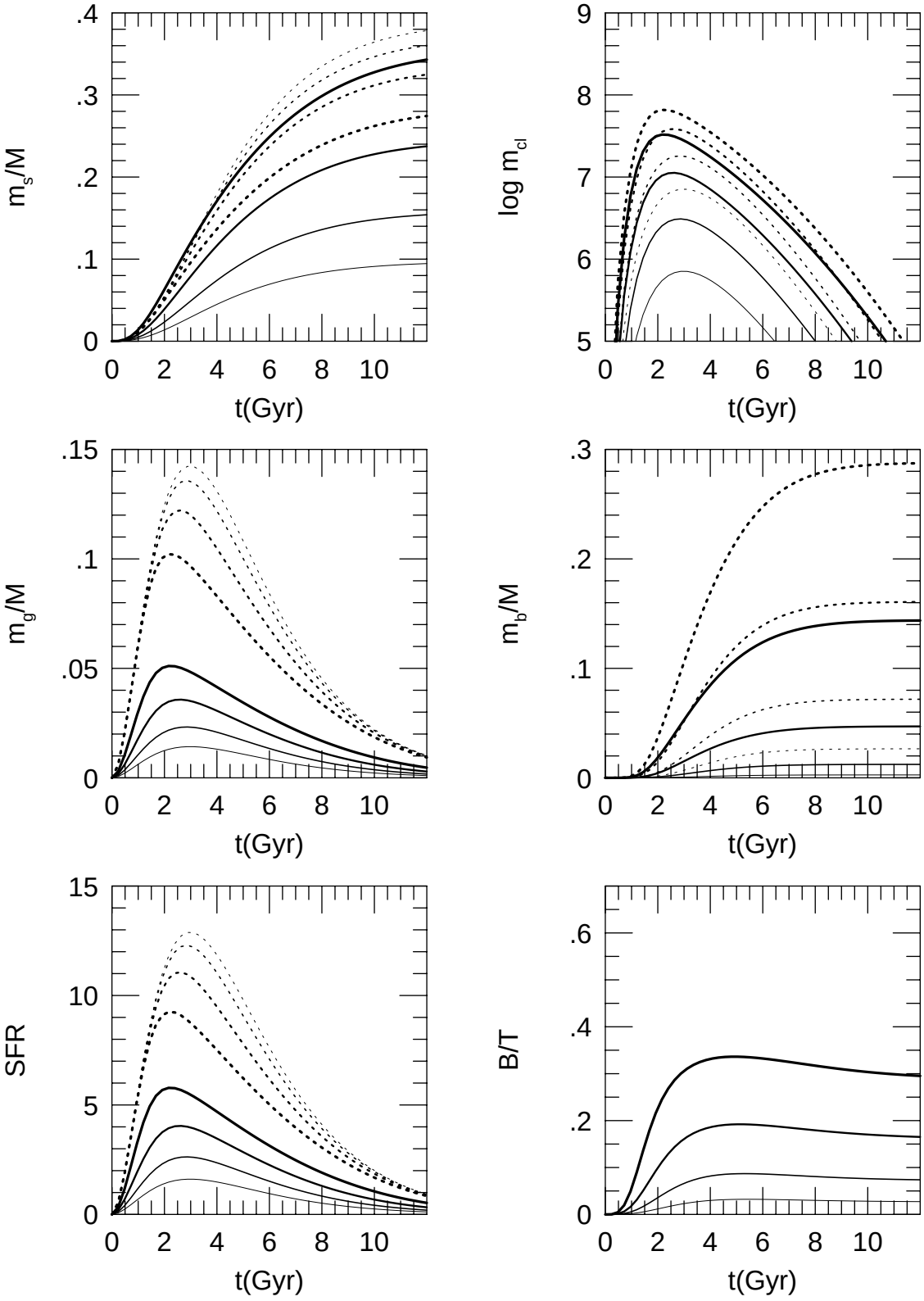
m_s/M
.4
.3
.2
.1
0
0 2 4 6 8 10
t(Gyr)
log m_cl
9
8
7
6
5
0 2 4 6 8 10
t(Gyr)
m_g/M
.15
.1
.05
0
0 2 4 6 8 10
t(Gyr)
m_b/M
.3
.2
.1
0
0 2 4 6 8 10
t(Gyr)
SFR
15
10
5
0
0 2 4 6 8 10
t(Gyr)
B/T
.6
.4
.2
0
0 2 4 6 8 10
t(Gyr)

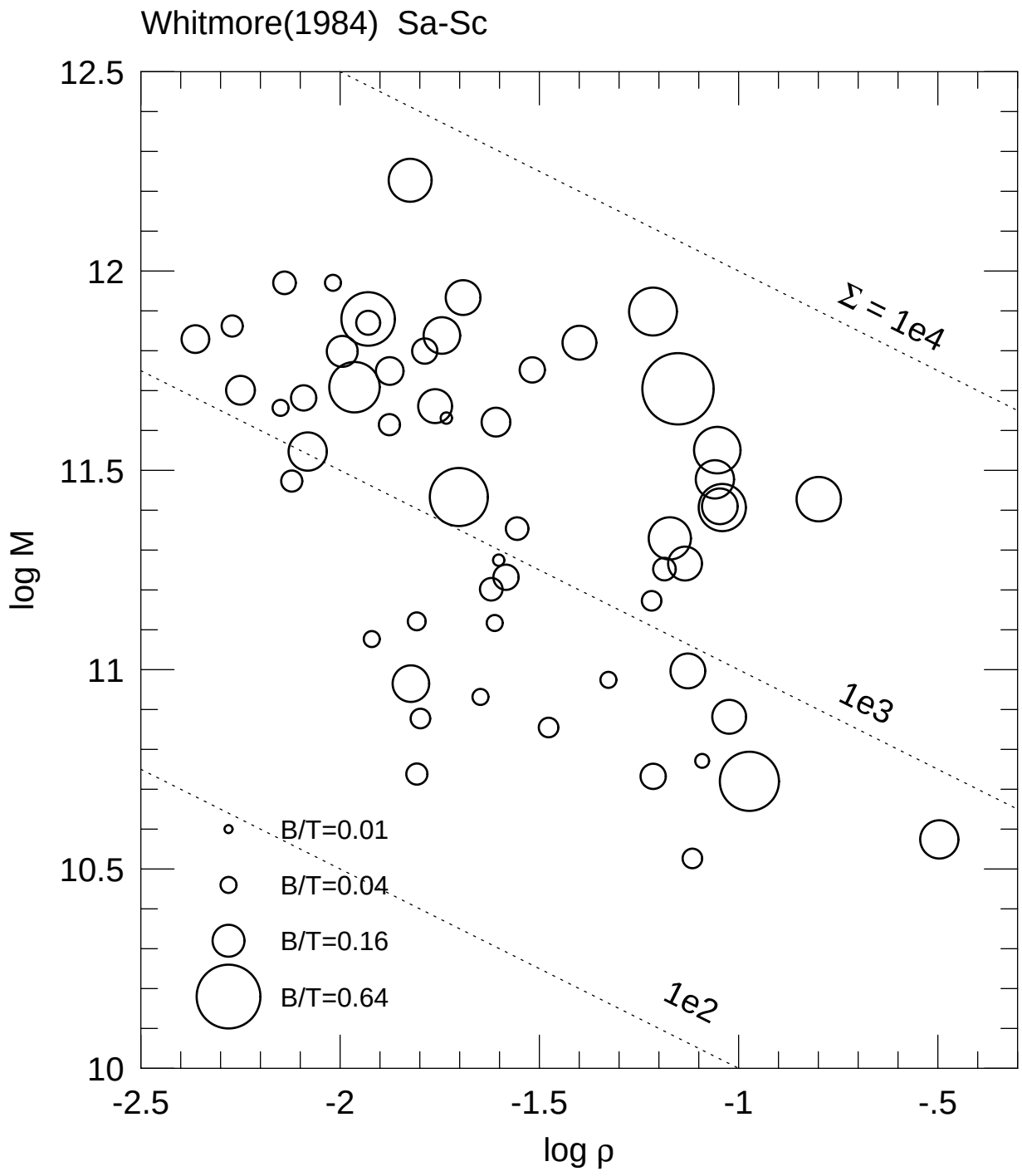
Whitmore(1984) Sa-Sc
12.5
12
11.5
11
10.5
10
log M
-2.5
-2
-1.5
-1
-.5
log ρ
Σ = 1e4
1e3
1e2
B/T=0.01
B/T=0.04
B/T=0.16
B/T=0.64

Whitmore(1984) Sa-Sc

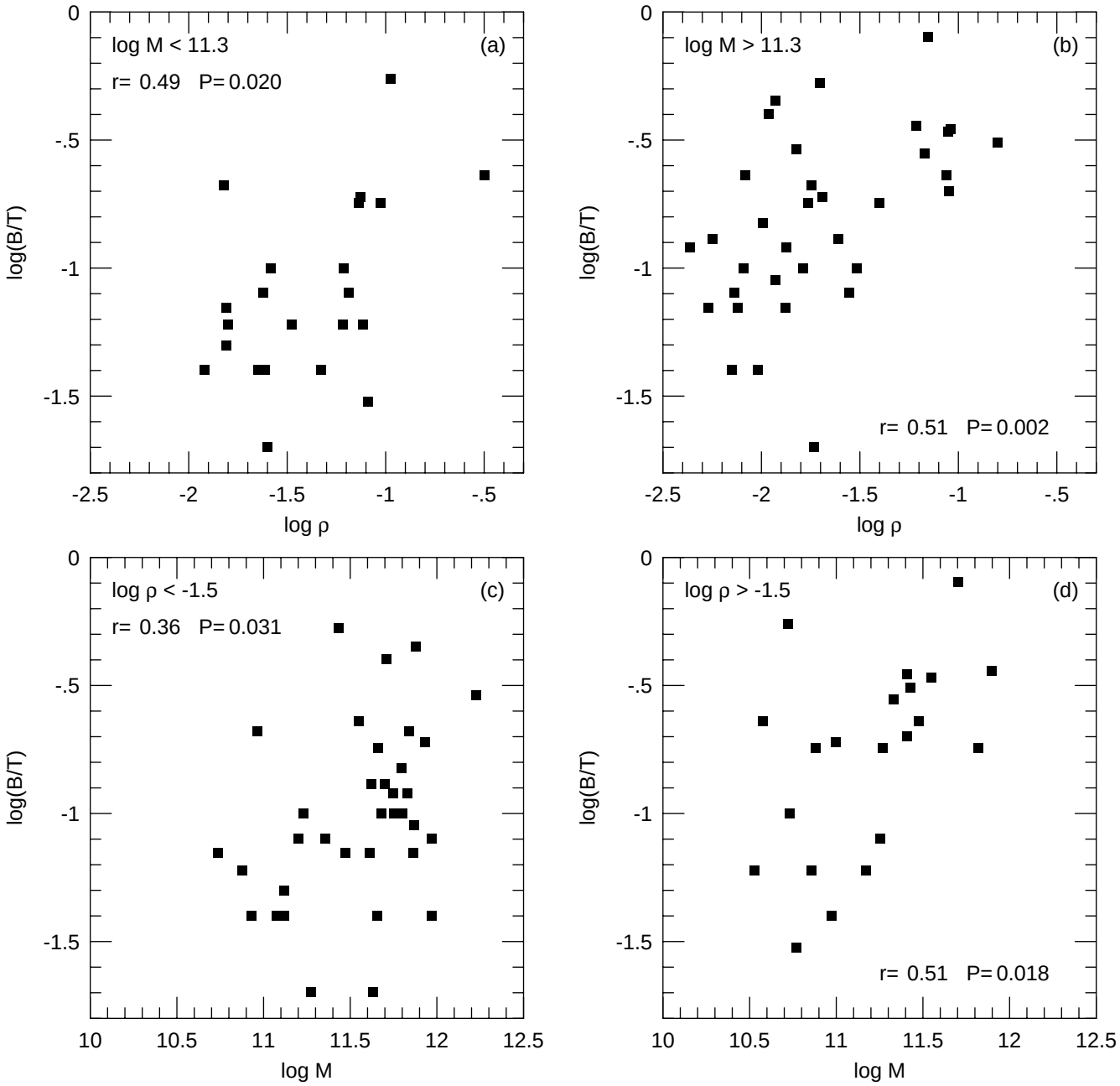

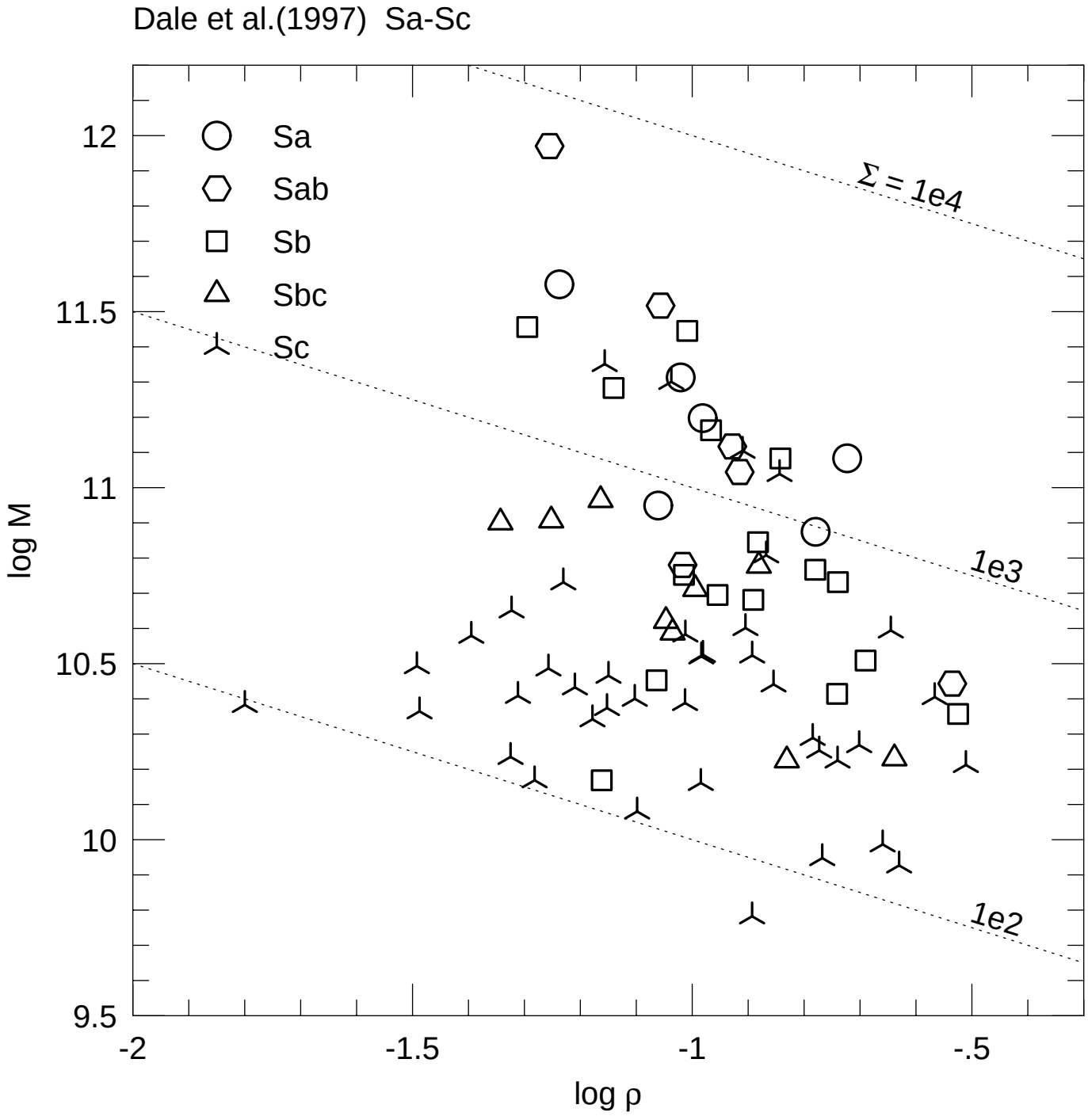
Dale et al.(1997) Sa-Sc
Sa
Sab
Sb
Sbc
Sc
Σ = 1e4
1e3
1e2
log M
log ρ
12
11.5
11
10.5
10
9.5
-2
-1.5
-1
-.5

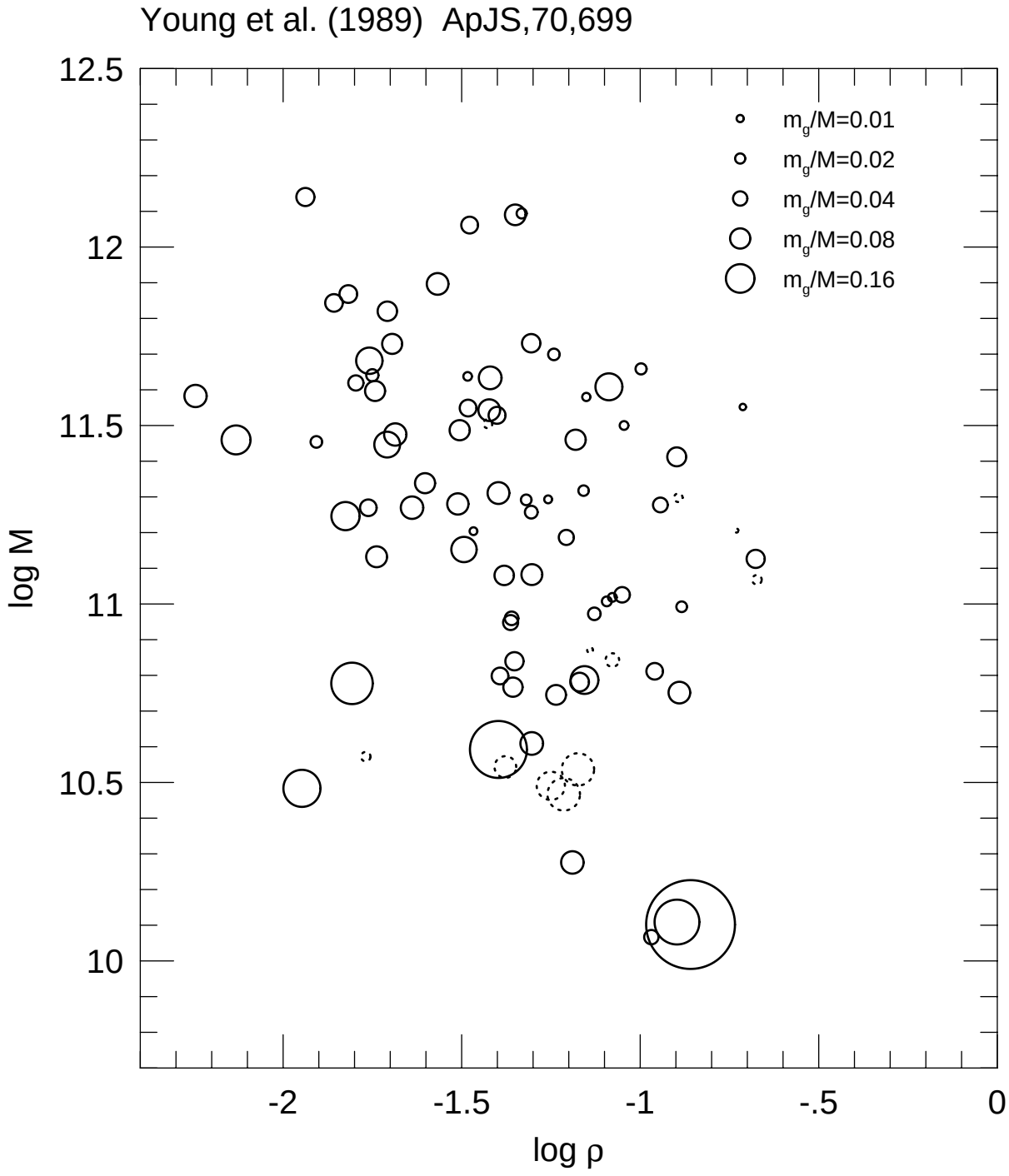
Young et al. (1989) ApJS,70,699
12.5
12
11.5
11
10.5
10
log M
-2
-1.5
-1
-.5
0
log ρ
m_g/M=0.01
m_g/M=0.02
m_g/M=0.04
m_g/M=0.08
m_g/M=0.16

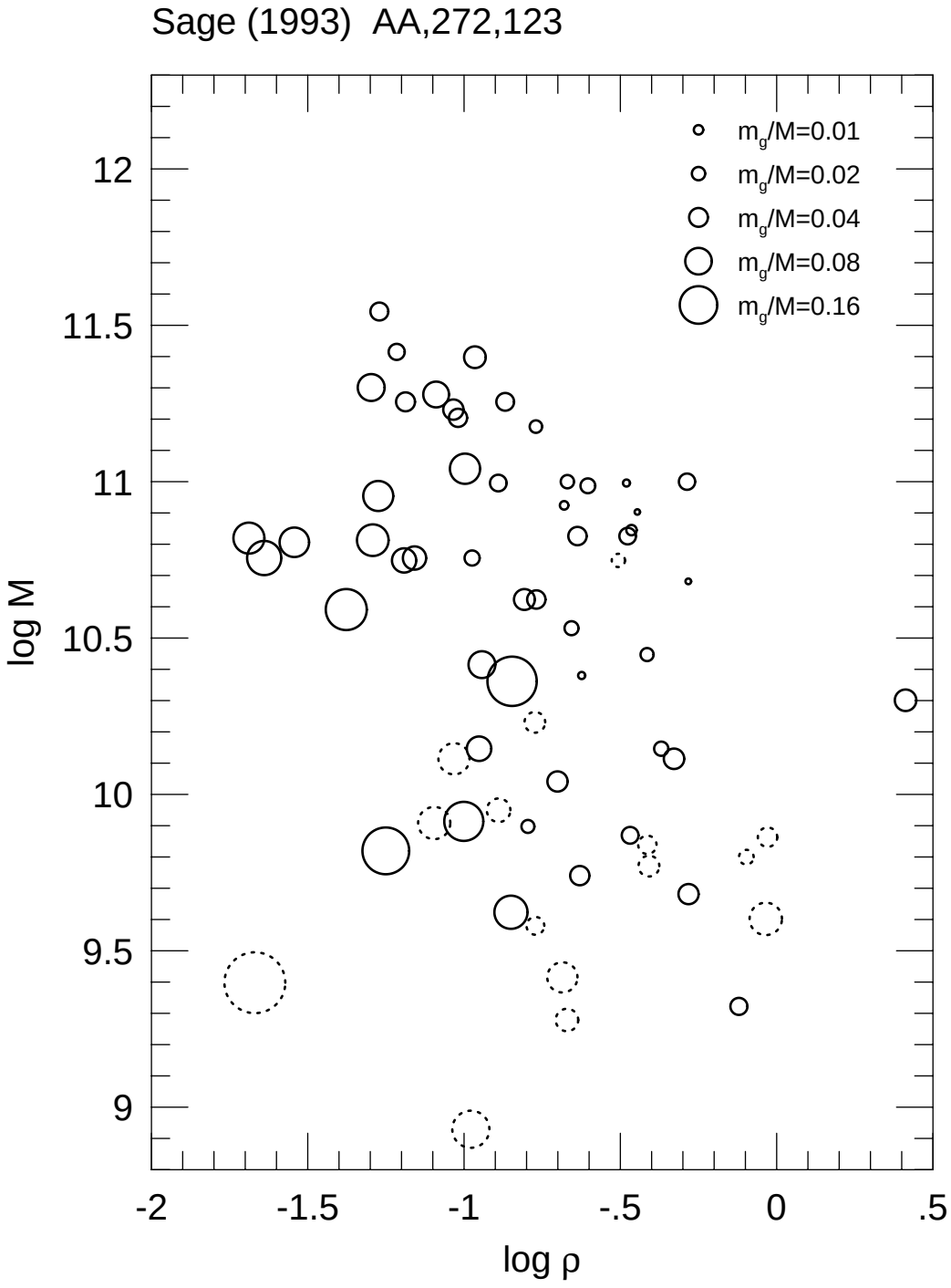
Sage (1993) AA,272,123
m_g/M=0.01
m_g/M=0.02
m_g/M=0.04
m_g/M=0.08
m_g/M=0.16
log M
12
11.5
11
10.5
10
9.5
9
-2
-1.5
-1
-.5
0
.5
log ρ

This figure "f13.gif" is available in "gif" format from:

http://arXiv.org/ps/astro-ph/9806355v1

This figure "f14.gif" is available in "gif" format from:

http://arXiv.org/ps/astro-ph/9806355v1

Γ(solid),β(dotted)

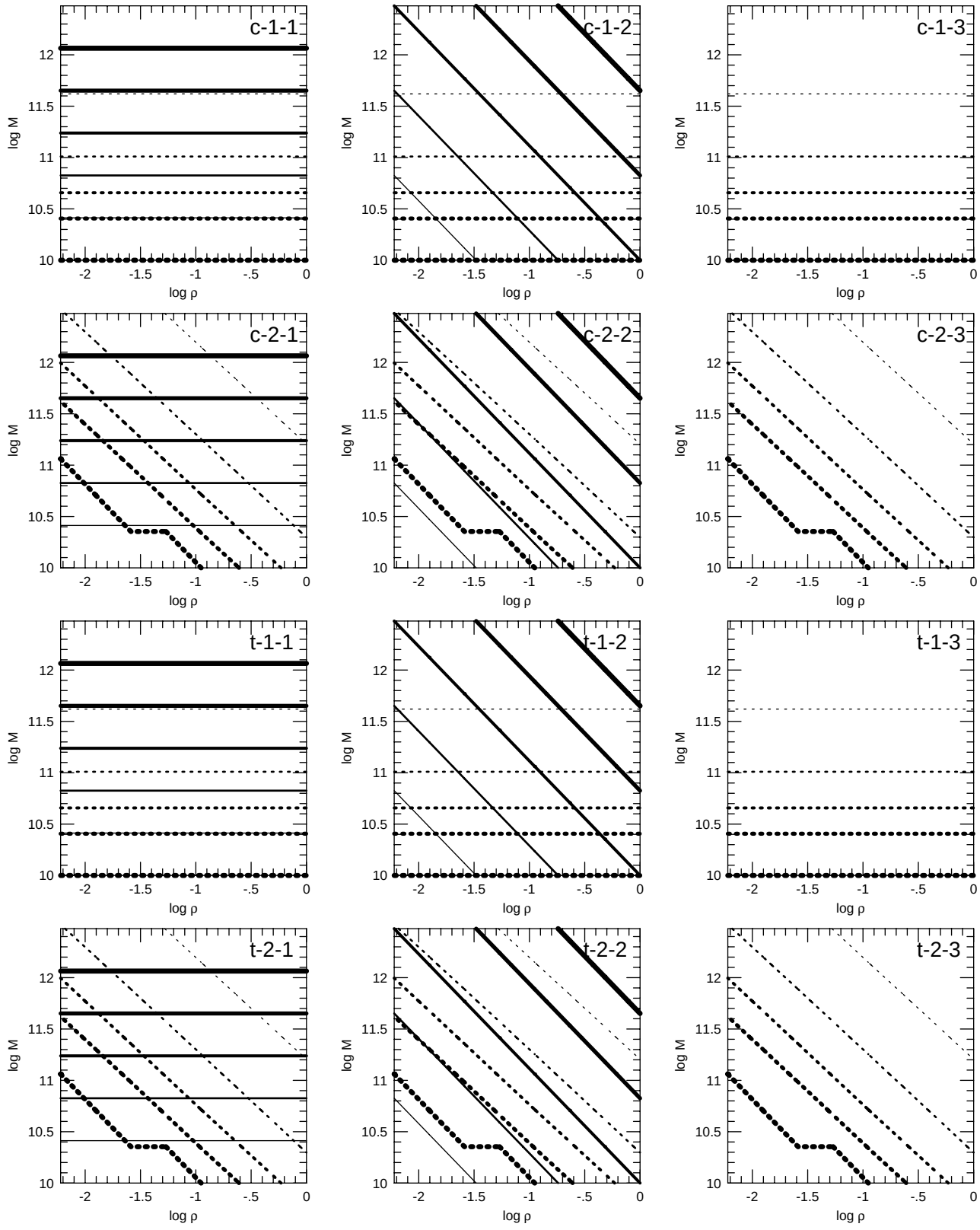

log(B/T)

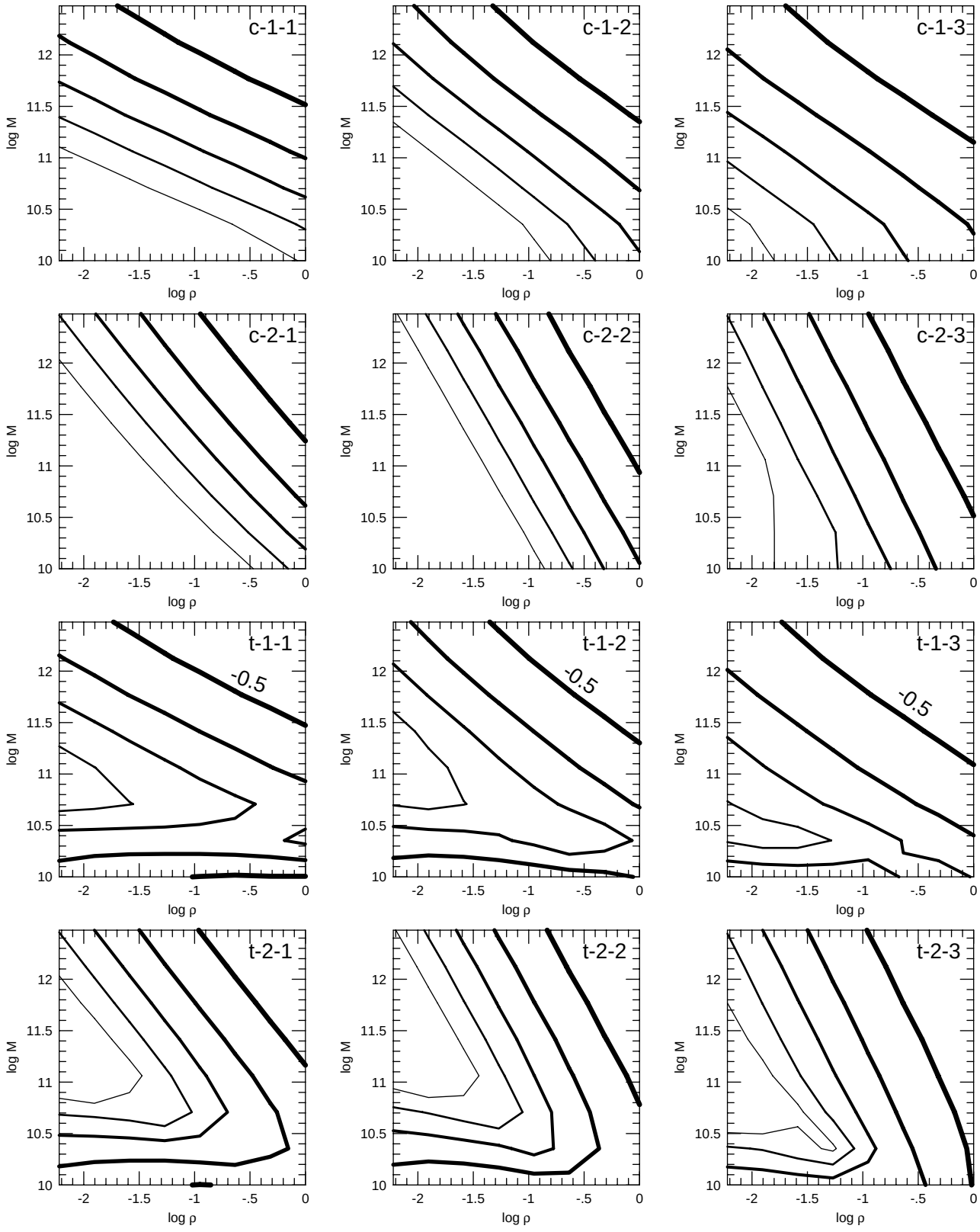
c-1-1
c-1-2
c-1-3
c-2-1
c-2-2
c-2-3
t-1-1
t-1-2
t-1-3
t-2-1
t-2-2
t-2-3
-0.5
log M
log ρ
12
11.5
11
10.5
10
-2
-1.5
-1
-.5
0

m_g/M

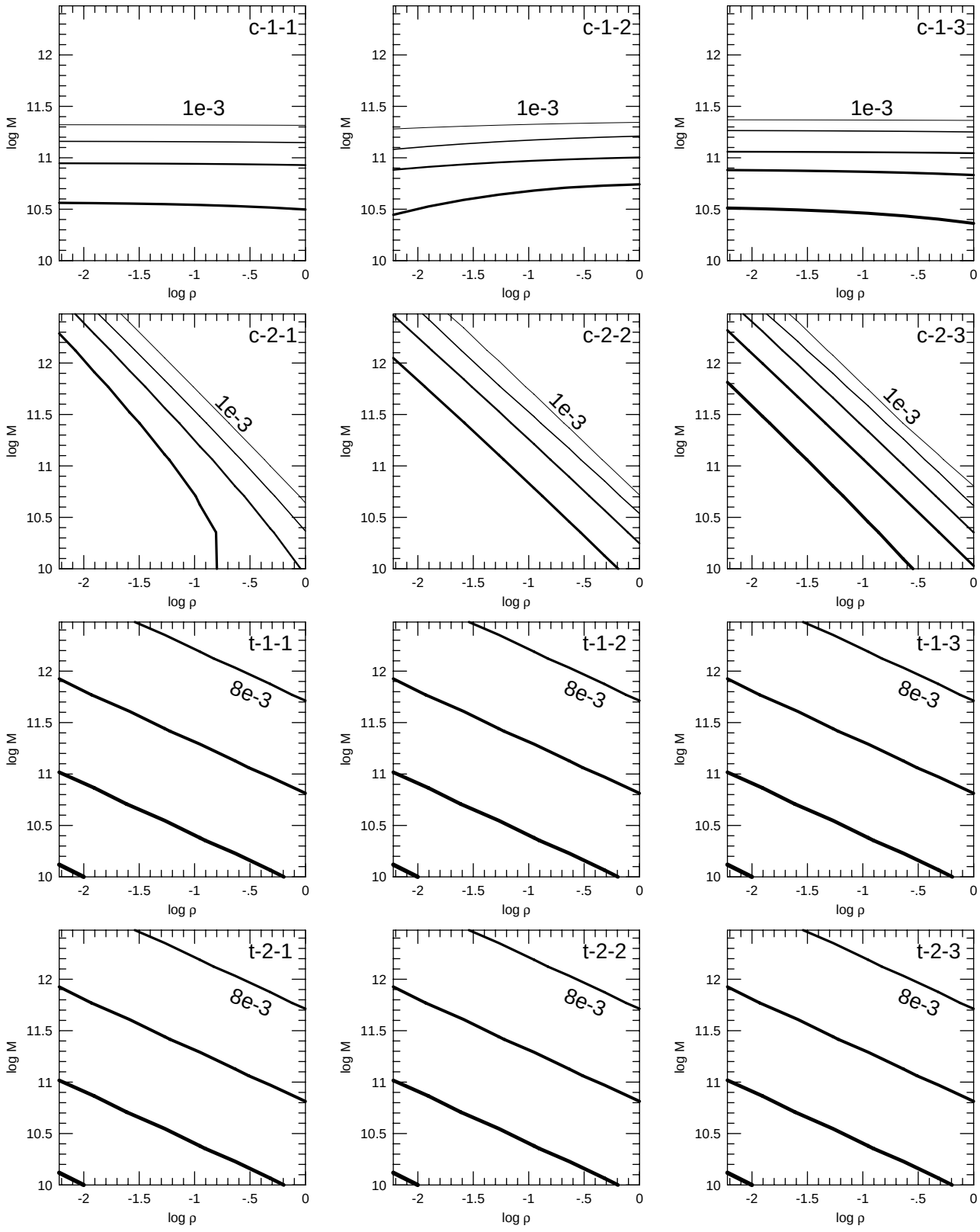
c-1-1
1e-3
c-1-2
1e-3
c-1-3
1e-3
c-2-1
1e-3
c-2-2
1e-3
c-2-3
1e-3
t-1-1
8e-3
t-1-2
8e-3
t-1-3
8e-3
t-2-1
8e-3
t-2-2
8e-3
t-2-3
8e-3
log M
log ρ
12
11.5
11
10.5
10
-2
-1.5
-1
-.5
0

SFR/M

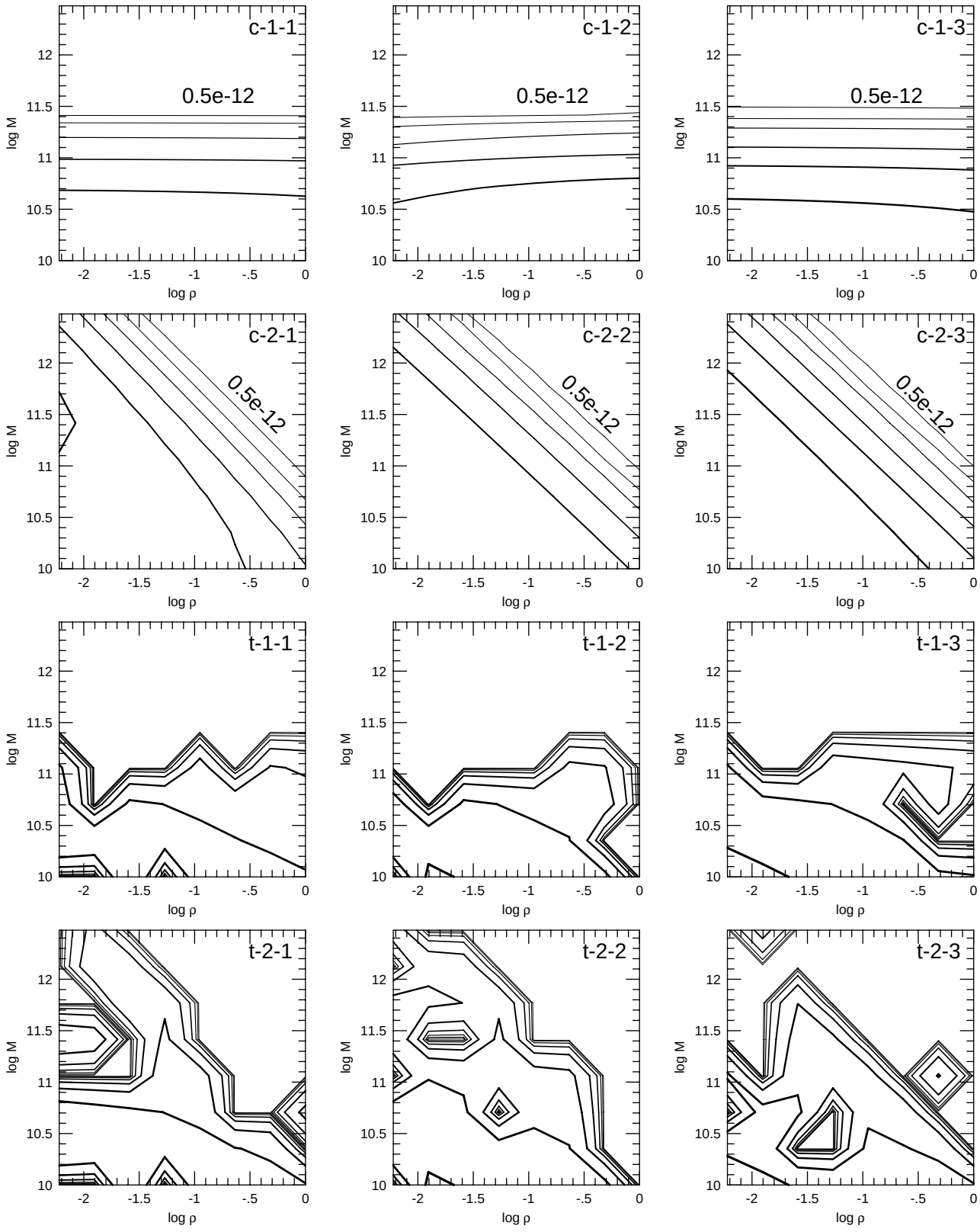
c-1-1
0.5e-12
c-1-2
0.5e-12
c-1-3
0.5e-12
c-2-1
0.5e-12
c-2-2
0.5e-12
c-2-3
0.5e-12
t-1-1
t-1-2
t-1-3
t-2-1
t-2-2
t-2-3
log M
log ρ
12
11.5
11
10.5
10
-2
-1.5
-1
-.5
0

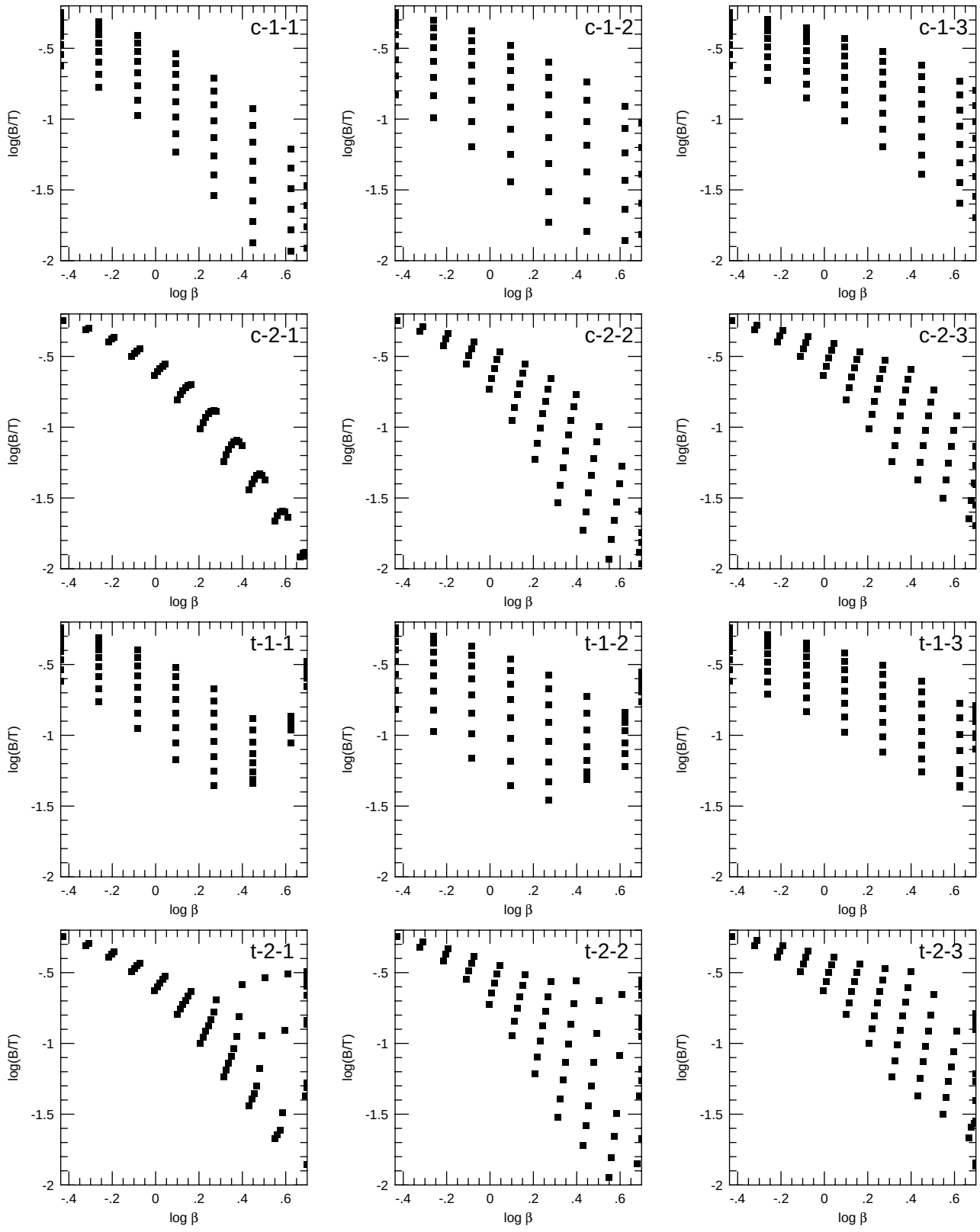
c-1-1
c-1-2
c-1-3
c-2-1
c-2-2
c-2-3
t-1-1
t-1-2
t-1-3
t-2-1
t-2-2
t-2-3
log(B/T)
log β
-.5
-1
-1.5
-2
-.4
-.2
0
.2
.4
.6

t_{bulge}

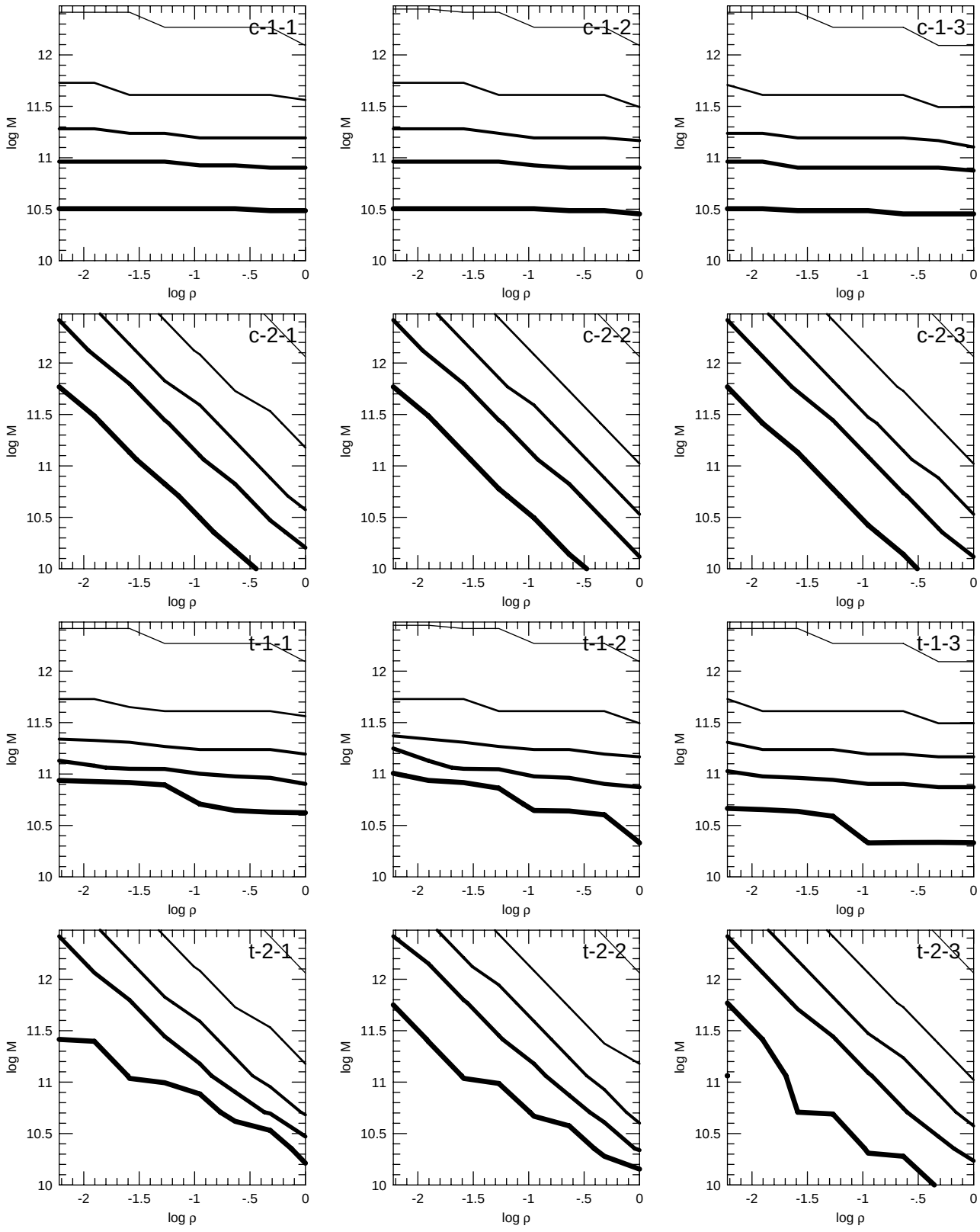
c-1-1
c-1-2
c-1-3
c-2-1
c-2-2
c-2-3
t-1-1
t-1-2
t-1-3
t-2-1
t-2-2
t-2-3
log M
log ρ
12
11.5
11
10.5
10
-2
-1.5
-1
-.5
0